AD_____

Award Number: DAMD17-99-1-9218

TITLE: Frequency-Domain Optical Mammograph

PRINCIPAL INVESTIGATOR: Sergio Fantini, Ph.D.

CONTRACTING ORGANIZATION: Tufts University
                          Medford, Massachusetts   02155

REPORT DATE: October 2000

TYPE OF REPORT: Annual

PREPARED FOR: U.S. Army Medical Research and Materiel Command
                Fort Detrick, Maryland   21702-5012

DISTRIBUTION STATEMENT: Approved for Public Release;
                        Distribution Unlimited

The views, opinions and/or findings contained in this report are
those of the author(s) and should not be construed as an official
Department of the Army position, policy or decision unless so
designated by other documentation.

20010404 131

REPORT DOCUMENTATION PAGE

1. AGENCY USE ONLY (Leave blank)	2. REPORT DATE October 2000	3. REPORT TYPE AND DATES COVERED Annual (1 Oct 99 - 30 Sep 00)	

4. TITLE AND SUBTITLE
Frequency-Domain Optical Mammograph

5. FUNDING NUMBERS
DAMD17-99-1-9218

6. AUTHOR(S)
Sergio Fantini, Ph.D.

7. PERFORMING ORGANIZATION NAME(S) AND ADDRESS(ES)
Tufts University
Medford, Massachusetts 02155

E-MAIL:
Sergio.fantini@tufts.edu

8. PERFORMING ORGANIZATION REPORT NUMBER

9. SPONSORING / MONITORING AGENCY NAME(S) AND ADDRESS(ES)

U.S. Army Medical Research and Materiel Command
Fort Detrick, Maryland 21702-5012

10. SPONSORING / MONITORING AGENCY REPORT NUMBER

11. SUPPLEMENTARY NOTES

12a. DISTRIBUTION / AVAILABILITY STATEMENT
Approved for public release; distribution unlimited

12b. DISTRIBUTION CODE

13. ABSTRACT (Maximum 200 Words)

This research project involves the analysis of a clinical data set of frequency-domain optical mammograms (~150 patients) to assess the performance of this approach to breast cancer detection. The analysis of the breast images is complemented by theoretical and experimental studies to characterize the proposed algorithms of image processing. The objective of this research is to identify the strengths and the weaknesses of the current instrument design, and to guide the design of new optical instrumentation for breast cancer detection.

During the first year of this research project, we have completed the initial analysis of the optical mammograms at each one of the four wavelengths used (690, 750, 788, 856 nm). The comparison of the single-wavelength optical mammograms with the pathology reports has led to building an ROC (Receiver Operating Characteristic) curve for this method. This ROC curve shows that single wavelength optical mammograms, while potentially sensitive to breast cancer, do not perform well in terms of discrimination of benign and malignant tumors. To exploit the spectral information, we have developed a perturbation approach to analyze the four-wavelength images, whose application to a subset of 19 patients has led to promising results. We are currently extending this analysis to a larger subset of data, and we are complementing it with alternative image-processing approaches.

14. SUBJECT TERMS
Optical Mammography, Mammography Screening, Near-Infrared Imaging, Photon Diffusion, Optical Tomography, Near-Infrared Tissue Spectroscopy

15. NUMBER OF PAGES
31

16. PRICE CODE

17. SECURITY CLASSIFICATION OF REPORT Unclassified	18. SECURITY CLASSIFICATION OF THIS PAGE Unclassified	19. SECURITY CLASSIFICATION OF ABSTRACT Unclassified	20. LIMITATION OF ABSTRACT Unlimited

Table of Contents

INTRODUCTION

This research project involves the analysis of an existing clinical set (~150 patients) of frequency-domain optical mammograms to assess the performance of this approach to breast cancer detection. The analysis of the breast images is complemented by theoretical and experimental studies to characterize the proposed algorithms of image processing. The objective of this research is to identify the strengths and the weaknesses of the current instrument design, and to guide the design of new optical instrumentation for breast cancer detection.

BODY

Approved statement of work

The approved statement of work for this project is the following:

Task 1.
Compute and analyze the edge-corrected optical mammograms for all 150 patients **(Months 1-18)**

    a. Install the optical mammography software for the SUN workstation;
    b. Build the edge-effect-corrected images (*N*-images) from the amplitude and phase images;
    c. Carry out a comparison between the *N*-images and the tumor diagnosis for each patient;
    d. Analyze the wavelength dependence of the *N* parameter and the ac amplitude for different kinds of tumors;
    e. Collect a printed summary of all the 2,400 *N*-images (150 patients, 2 breasts, 2 projections, 4 wavelengths) and the spectral features of all the tumors.

Task 2.
Perform the optical measurements on breast-like phantoms **(Months 19-24)**

    a. Prepare the breast-like phantoms (optical inhomogeneities + strongly scattering background);
    b. Collect and analyze the optical data;
    c. Repeat the experiment for a variety of sizes, shapes, optical contrasts, and inhomogeneous backgrounds.

Task 3.
Apply the method for the quantification of the tumor optical properties and construct the spectral chart for benign and malignant tumors **(Months 25-36)**

    a. Find the optical properties, and the hemoglobin-related parameters of the tumors;
    b. Build charts of benign and malignant regions in the μ_a-μ_s' plane at four wavelengths;
    c. Determine whether malignant tumors show a specific spectral signature.

The first Grant period (year 01) was devoted to Task 1 (which was planned for the first 18 months of the project). The accomplishments relative to each one of the sub-tasks are described below.

Task 1.a.

The software provided by Siemens for the display of the optical mammograms has been installed on the SUN workstation. This step did not present any problem, as the software developed by Siemens was compatible with the new SUN operating system.

Task 1.b.

The software has been modified to allow for the computation of the N images from the amplitude and phase images. We briefly recall that the so-called N images are the result of an algorithm of image processing previously developed by us to minimize the effect of the breast thickness variability on the optical mammograms [Fantini et al., 1996]. The N images enhance the tumor detectability with respect to amplitude or phase images. The details of the image processing algorithm leading to the N-images can be found in the appended publication by Fantini et al., 1996 (Medical Physics, vol.23). In particular, the modified software implements a versatile approach that allows the user to select the values of the parameters required to compute the N image (reference pixel, average optical properties of breast tissue, etc.). A representative case, N-image at 850 nm, is shown in Fig. 1. The case in Fig. 1 refers to a 71 year-old patient affected by breast cancer. The cancer, 3 cm in diameter, is clearly detected in both views of the left breast (LC: left craniocaudal; LO: left oblique).
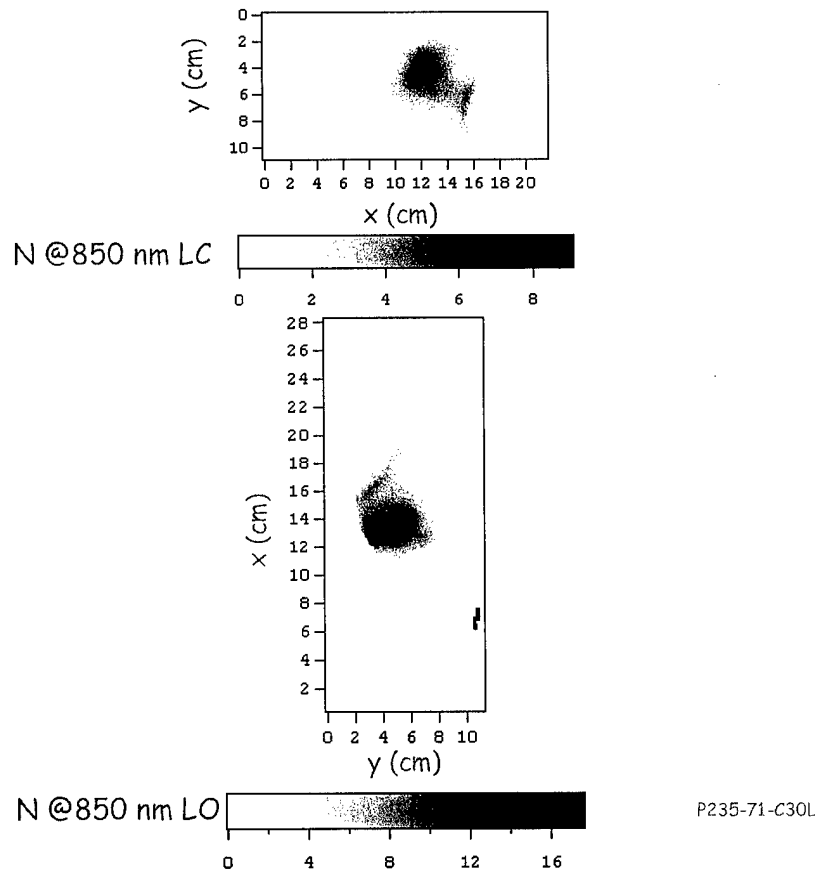
Fig. 1. Representative N-images of the left breast of a 71 year-old patient affected by cancer. The two images refer to the craniocaudal (LC) and oblique (LO) projections. The 3 cm cancer is clearly detected in both views as a region of higher absorbance (dark area).

The software displays the N-images for the four wavelengths used (690, 750, 788, 856 nm), and saves the images as ASCII files for further processing. An example of the four N-images, one per wavelength, of the same breast is shown in Fig. 1. This figure shows that the cancer (in the center of the image) and the blood vessels (identified by their thread-like shape) may show different spectral trends. In fact, in this case the cancer contrast decreases with wavelength, while the contrast of blood vessels increases with wavelength.
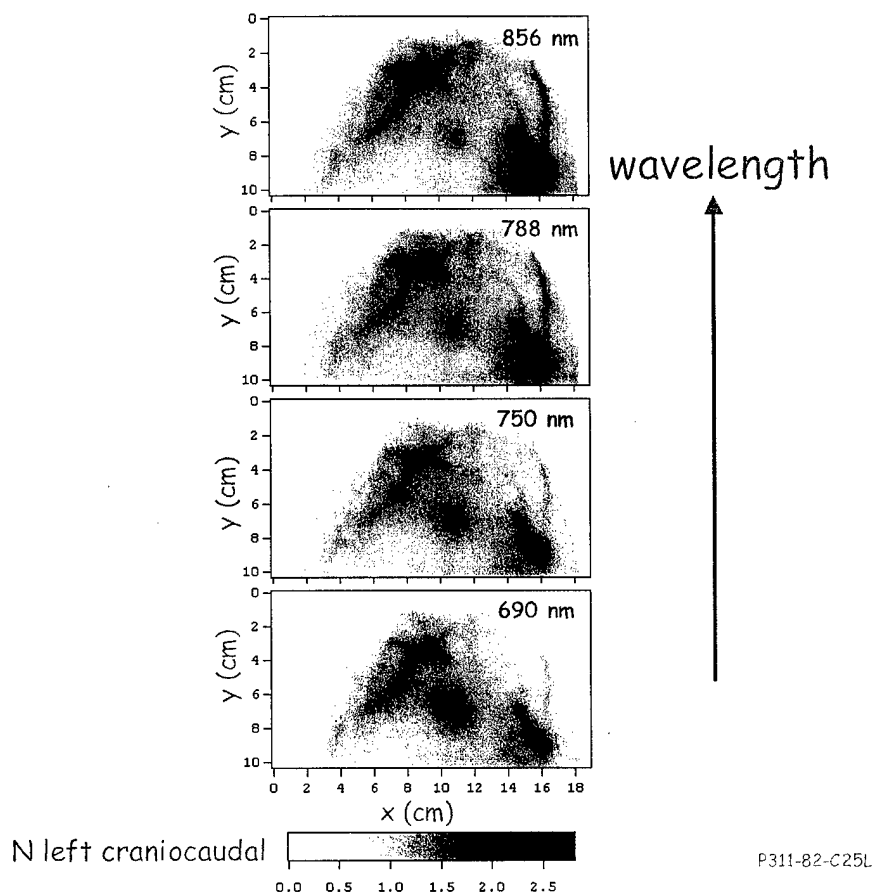

Fig. 2. N images at four wavelengths for the left breast, craniocaudal projection, of an 82 year-old patient affected by cancer. The cancer, 2.5 cm in size, is detected at the center of the image. The other optical inhomogeneities, darker areas, are assigned to blood vessels due to their morphology. The relative contrast of the cancer and the blood vessels changes with wavelength.

Task 1.c.
We have computed and printed the N-images for the 131 patients for which we had a complete pathology report. We have carefully evaluated these N-images, and compared the optical diagnosis with the actual diagnosis. Initially, we have considered an optical mammogram to be positive only if an abnormal region (dark area) appears in both projections of the same breast. Following this criterion, we have found the results shown in Fig. 3.

sensitivity:
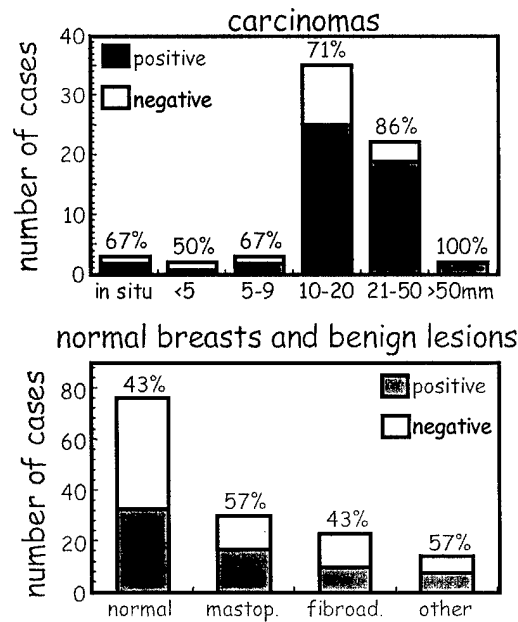TP/(TP+FN) = 76%

specificity:
TN/(TN+FP) = 52%

Fig. 3. Summary of the positive and negative optical mammograms analyzed according to the criterion that an optical mammogram is positive if a suspicious area is detected in both views of the same breast. The upper panel refers to cancerous breasts, while the lower panel refers to healthy breasts and breasts with benign lesions. The resulting sensitivity and specificity are listed.

We have also applied different criteria, in order to build an ROC (Receiver Operating Characteristic) curve for the diagnostic approach afforded by single-wavelength N-images. The various criteria for positivity were based on requiring that a suspicious region be detected in both views, in at least one view, with a contrast beyond a given threshold, or such that the suspicious area does not have a symmetrical counterpart in the contralateral breast. As a result, we have built the ROC curve shown in Fig. 4. This ROC curve is very similar to the one originally reported by the Siemens group [Götz et al., 1998], but there is one remarkable difference. The ROC curve of Fig. 4 has been obtained using optical mammograms at one wavelength, while the Siemens group used data at two wavelengths to build their ROC curve. Therefore, we hope to further improve upon the ROC curve of Fig. 4, by exploiting the multi-wavelength data available to us.
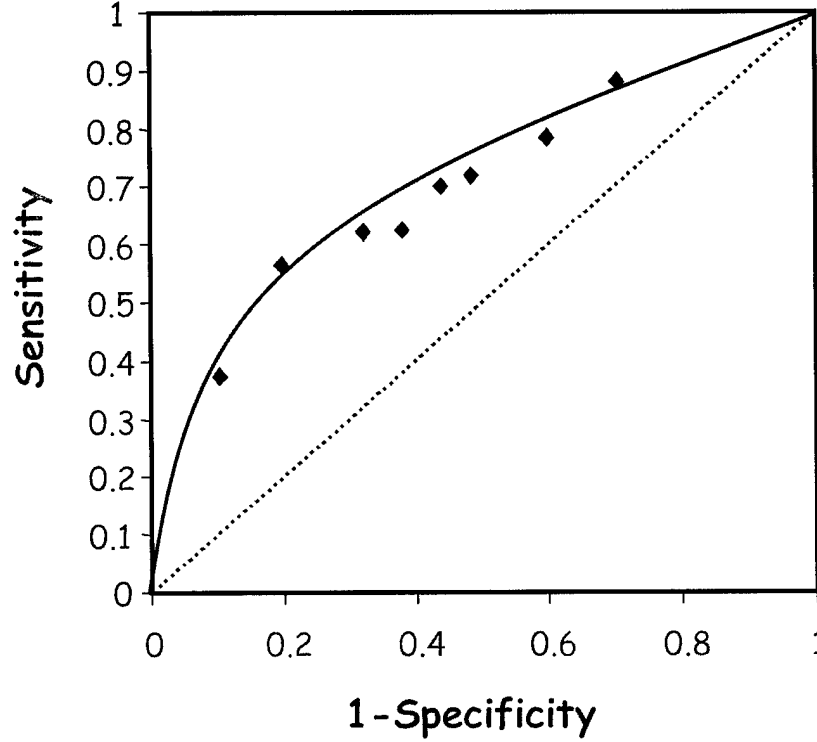
7

Fig. 4. ROC curve obtained from the N-images at one wavelength (690 nm) on a clinical population of 131 patients.

Task 1.d.

For the study of the wavelength dependence of suspicious areas detected in the optical mammograms, we have initially implemented a feature in the software that imposes the same reference pixel for the computation of the N image at all wavelengths. We felt that this is important to guarantee that the data at each wavelength has a common reference point. Then, we have developed a perturbation approach, based on diffusion theory, to assign an absorption perturbation to each optical inhomogeneity detected in the breast. This perturbation approach is based on the fact that the absorption perturbation $\Delta\mu_a$ (to within an unknown wavelength independent factor C) can be written as:

$$C\Delta\mu_a(\lambda) = \frac{1}{\mu'_{s0}(\lambda)} \cdot \frac{\Delta I}{I_0}(\lambda)$$

(1)

where μ_{s0}' is the average reduced scattering coefficient of healthy breast tissue, I_0 is the unperturbed optical intensity, and ΔI is the measured intensity perturbation. Finally, we have fitted the spectrum of the absorption perturbation with a linear combination of the extinction spectra of oxy- and deoxy-hemoglobin. By considering the oxy- and deoxy-hemoglobin concentrations ([HbO$_2$] and [Hb], respectively) as fitting parameters, we can translate the spectral information into the tumor oxygenation (given by [HbO$_2$]/([Hb]+[HbO$_2$])). This approach is depicted in Fig. 5 for the same case shown in Fig. 1.
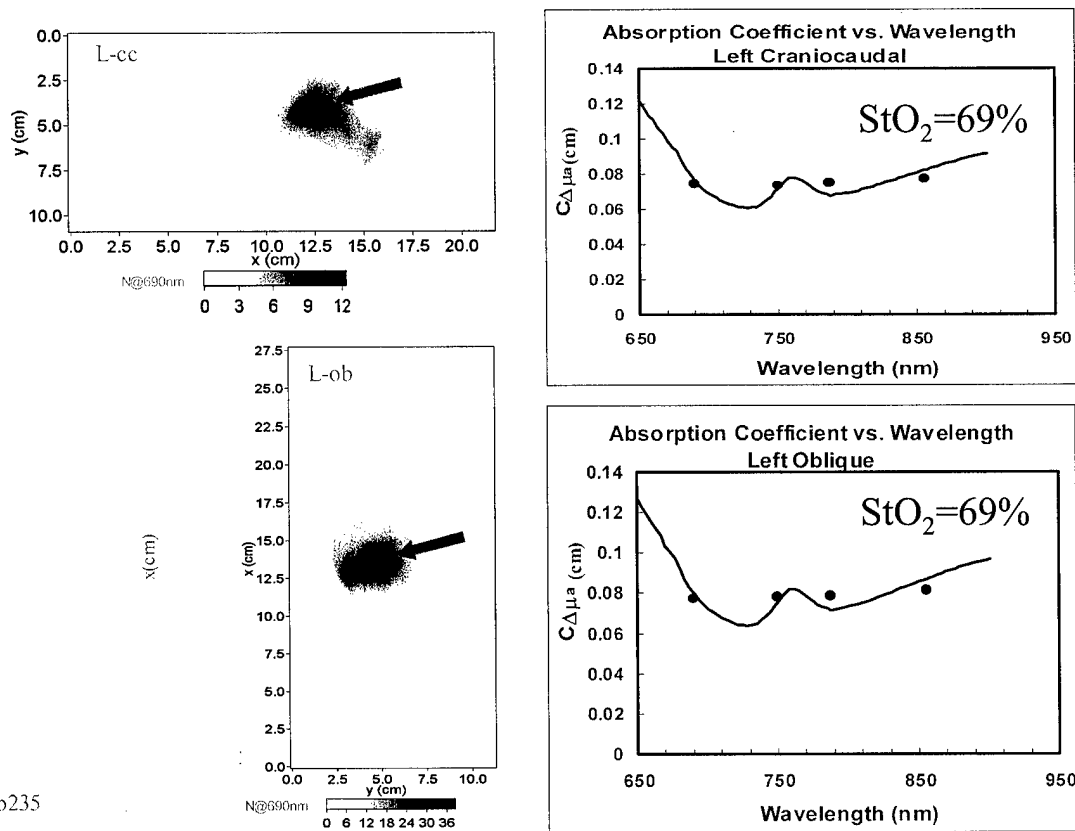
Fig. 5. The application of a perturbation approach assigns the absorption perturbation $\Delta\mu_a$ (to within an unknown wavelength independent factor, C) to a detected optical inhomogeneity (indicated by the arrow in the image). By fitting the absorption spectrum with the hemoglobin spectrum, we can assign a tissue saturation value (StO_2) to the detected inhomogeneity. The unknown factor C cancels out in this process (because a multiplicative factor in the absorption spectrum does not affect the tissue saturation value).

We have applied this perturbation approach to a subset of 19 patients, obtaining promising results in terms of spectral discrimination of benign and malignant breast lesions. These results are illustrated in Fig. 6.
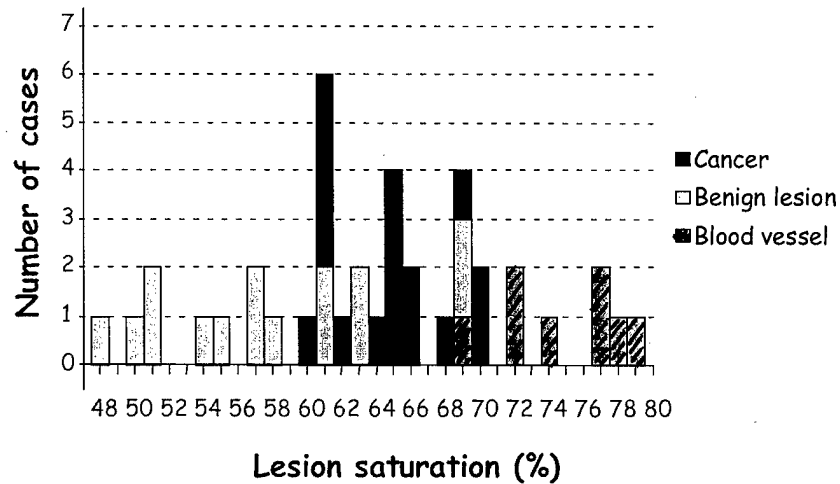
9

Fig. 6. Oxygen saturation of the hemoglobin in various detected breast lesions (cancers, benign tumors, blood vessels). The lesion saturation, which reflects the spectral behavior of the corresponding absorption, may help discriminating cancer from benign lesions.

The result that malignant lesions have a higher oxygenation than benign tumors (see Fig. 6) is surprising. Before trying to interpret the physiological meaning of this result, however, we need to better characterize the perturbation approach used to obtain Fig. 6. To this aim, we are currently performing a theoretical study and we are starting to design the experimental study planned in Task 2.

A difficulty we are facing is related to the fact that we reference each N-image to a specific pixel in the mammogram (in fact, a reference pixel is required to compute the N-image). This means that the spectral dependence of N is not just affected by the spectral dependence of the tumor, but also by the spectral dependence of the reference pixel. Our first approach to tackle this problem has been to take an average measurement of the intensity I over the whole breast as a reference reading (i.e. I_0 in Eq. (1)) for the perturbation approach described above. This may reduce the variability of the spectral dependence of the reference reading. We are currently in the process of quantifying the effectiveness of this averaging approach.

Task 1.e.
We have already collected a printed summary of the N-images computed for the whole clinical data set provided by Siemens. Currently, we have analyzed the spectral information of a subset of 19 patients, and we are currently continuing the spectral analysis, based on the perturbation approach, on a larger data set. We are also considering a modified perturbation approach, as well as other image processing approaches.

KEY RESEARCH ACCOMPLISHMENTS

- Implemented modifications to the software for the computation of N-images and for the computation of the tumor contrast for each optical mammogram.
- Computation of the N-images for the whole data set of ~150 patients.
- Determination of the ROC diagram based on one-wavelength N images for the 131 patients with complete pathology report.

- Development of a perturbation approach for the spectral analysis of the optically detected breast lesions.
- Determination of the effectiveness of the spectral perturbation approach to discriminating benign and malignant breast lesions on a subset of 19 patients.

REPORTABLE OUTCOMES

Manuscripts (three copies of these manuscripts are enclosed with this report)
S. Fantini, E. L. Heffer, M. A. Franceschini, L. Götz, A. Heinig, S. Heywang-Köbrunner, Oliver Schütz, and Horst Siebold, "Optical Mammography with Intensity-Modulated Light," Proceedings Volume from In Vivo Optical Imaging Workshop (September 16-17, 1999, National Institutes of Health, Bethesda, MD), A. Gandjbakhche, Ed. (Optical Society of America, Washington, DC, 2000), *in press*.

E. L. Heffer, M. A. Franceschini, S. Heywang-Köbrunner, L. Götz, A. Heinig, O. Schütz, H. Siebold, and S. Fantini "Analysis of Frequency-Domain Optical Mammograms Using Spectral Information," OSA *Trends in Optics and Photonics (TOPS) Vol. 38, Biomedical Topical Meetings*, Technical Digest, Postconference Edition (Optical Society of America, Washington, DC, 2000), pp. 401-402.

Presentations
S. Fantini, "Optical Mammography," Department of Electrical Engineering and Computer Science, Tufts University, Medford, MA, November 10, 1999.

E. L. Heffer, M. A. Franceschini, S. Fantini, S. Heywang-Köbrunner, L. Götz, A. Heinig, Oliver Schütz, and Horst Siebold, "Analysis of Frequency-Domain Optical Mammograms Using Spectral Information," OSA Biomedical Topical Meeting, Miami, FL, April 2-5, 2000.

S. Fantini, "Using intensity-modulated light top detect breast cancer," Center for Innovative Minimally Invasive Therapy (CIMIT), Massachusetts General Hospital, Boston, MA, May 2, 2000.

E. L. Heffer, "Spectral Analysis of Frequency-Domain Optical Mammograms," Beckman Laser Institute, University of California at Irvine, May 12, 2000.

E. L. Heffer, M. A. Franceschini, O. Schütz, H. Siebold, L. Götz, A. Heinig, S. Heywang-Köbrunner, and S. Fantini "Analysis of Frequency-Domain Optical Mammograms Using Spectral Information," Gordon Conference on *Lasers in Medicine and Biology*, New London, CT, June 10-15, 2000.

CONCLUSIONS

We have completed the initial analysis of the optical mammograms based on the N-images at the four wavelengths used. This analysis has led to the ROC curve reported in Fig. 4. We have started the proposed study of the spectral dependence of the optically detected tumors. To this aim, we have developed a perturbation approach, whose application to a subset of 19 patients has led to the results reported in Fig. 6. We plan to continue this analysis, and to complement it with alternative approaches.

The relevance of our results is that single wavelength N-images (Fig. 4) are as effective as a previously reported two-wavelength analysis. We hypothesize that by exploiting the additional information provided by four-wavelength data, we can further improve the performance of frequency-domain optical mammography. This is the focus of our current research activity related to this project.

REFERENCES

Fantini, S., M. A. Franceschini, G. Gaida, E. Gratton, H. Jess, W. W. Mantulin, K. T. Moesta, P. M. Schlag, and M. Kaschke, "Frequency-Domain Optical Mammography: Edge Effect Corrections," Med. Phys. **23**, 149-157 (1996).

Götz, L., S. H. Heywang-Köbrunner, O. Schütz, and H. Siebold, "Optische Mammographie an Präoperativen Patientinnen," Akt. Radiol. **8**, 31-33 (1998).

APPENDIX

The appendix contains a copy of the following article describing the algorithm to compute the edge-corrected N-images:

Fantini, S., M. A. Franceschini, G. Gaida, E. Gratton, H. Jess, W. W. Mantulin, K. T. Moesta, P. M. Schlag, and M. Kaschke, "Frequency-Domain Optical Mammography: Edge Effect Corrections," Med. Phys. **23**, 149-157 (1996).

Frequency-domain optical mammography: Edge effect corrections

Sergio Fantini and Maria Angela Franceschini
Laboratory for Fluorescence Dynamics, Department of Physics, University of Illinois at Urbana–Champaign, 1110 West Green Street, Urbana, Illinois 61801-3080

Gerhard Gaida
Carl Zeiss, Medical-Optical Instruments, D 73446 Oberkochen, Germany

Enrico Gratton
Laboratory for Fluorescence Dynamics, Department of Physics, University of Illinois at Urbana–Champaign, 1110 West Green Street, Urbana, Illinois 61801-3080

Helge Jess
Carl Zeiss, Medical-Optical Instruments, D 73446 Oberkochen, Germany

William W. Mantulin
Laboratory for Fluorescence Dynamics, Department of Physics, University of Illinois at Urbana–Champaign, 1110 West Green Street, Urbana, Illinois 61801-3080

K. Thomas Moesta and Peter M. Schlag
Robert Roessle Hospital and Tumor Institute, Humbolt University, D 13122 Berlin, Germany

Michael Kaschke
Carl Zeiss, Medical-Optical Instruments, D 73446 Oberkochen, Germany

We have investigated the problem of edge effects in laser-beam transillumination scanning of the human breast. Edge effects arise from tissue thickness variability along the scanned area, and from lateral photon losses through the sides of the breast. Edge effects can be effectively corrected in frequency-domain measurements by employing a two-step procedure: (1) use of the phase information to calculate an effective tissue thickness for each pixel location; (2) application of the knowledge of tissue thickness to calculate an edge-corrected optical image from the ac signal image. The measurements were conducted with a light mammography apparatus (LIMA) designed for feasibility tests in the clinical environment. Operating in the frequency-domain (110 MHz), this instrument performs a transillumination optical scan at two wavelengths (685 and 825 nm). We applied the proposed two-step procedure to data from breast phantoms and from human breasts. The processed images provide higher contrast and detectability in optical mammography with respect to raw data breast images. © *1996 American Association of Physicists in Medicine.*

Key words: optical mammography, transillumination, laser beam scanning, breast tumor, frequency-domain

I. INTRODUCTION

Among the various potential applications of optical imaging of biological tissue, the investigation of breast cancer is one of the most promising. Breast transillumination with continuous wave (CW) light was first proposed in 1929 to detect breast lesions.[1] This CW, broad-beam transillumination methodology, also called diaphanography or lightscanning, has been thoroughly investigated in the past two decades to address its feasibility and effectiveness.[2-8] The main difficulty with optical mammography arises from the strongly diffusive nature of light propagation in breast tissue. This feature reduces contrast[8] and resolution[9] of optical images, thus limiting the sensitivity of the method for small and deep tumors.[6,8] Higher sensitivity can be achieved with collimated, narrow-beam transillumination,[10] which delivers a narrow interrogating laser beam on one side of the breast and employs a localized detector on the other.[11,12] Recently, time-resolved methods have been developed to provide data with higher information content than the simple intensity attenuation provided by CW techniques. These time-resolved methods work in either the time-domain or the frequency-domain. In the time-domain, one measures the transformation of a short light pulse (typically a few picoseconds FWHM) traversing the tissue.[13,14] In the frequency domain, the intensity of the light source is modulated at a frequency on the order of 10^8 Hz, and the measured quantities are the phase shift and amplitude attenuation of the tissue transmitted intensity wave.[15-20] In the time-domain, it is possible to apply a time-gate to the detector to select photons which have traveled shorter path lengths.[21-23] Time gating improves the image contrast and resolution.[24,25] In the frequency-domain, a similar result can be achieved by employing high modulation frequencies.[26,27] However, improvement in contrast and resolution is obtained at the expense of a decreased signal-to-noise ratio due to the low signal from weakly scattered photons. Consequently, to maximize image quality, one seeks the best compromise between the requirements of improved contrast/resolution, and a high signal-to-noise ratio. In general, the higher information content of time resolved measurements can be used to
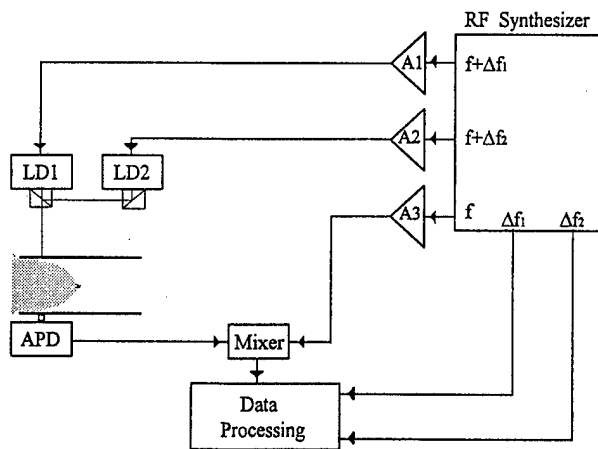
FIG. 1. Schematic diagram of the frequency-domain light mammography apparatus (LIMA). A1, A2, A3 are radio frequency amplifiers; LD1 and LD2 are laser diodes emitting at 685 and 825 nm, respectively; APD is an avalanche photodiode; $f=110$ MHz; $\Delta f_1=1$ kHz; $\Delta f_2=0.8$ kHz.

separate and quantify absorption and scattering contributions to intensity attenuation.[14,28] In the future, this capability may lead to functional imaging, or to highly specific optical mammography. As an alternative, the additional information can be used to treat geometrical effects (such as breast thickness variation within the scanned region) and/or boundary conditions. In this paper we have followed the latter approach.

This article presents a frequency-domain light mammography apparatus (LIMA) that performs laser-beam transillumination of the breast. Our objective is to produce the highest possible image contrast. To this end, we investigate the problem of determining a parameter, derived from the frequency-domain raw data, that enhances the detectability of optical inhomogeneities in the breast. In particular, this parameter should correct for effects related to tissue thickness variability within the scanned region, and to photon losses through the sides of the breast. We have performed laboratory measurements on breast simulating phantoms to test the effectiveness of our derived parameter. Finally, we have applied our method to clinical data obtained with the frequency-domain light mammography apparatus.

II. LIGHT MAMMOGRAPHY APPARATUS (LIMA)

A schematic diagram of the frequency-domain light mammography apparatus (LIMA) is shown in Fig. 1. This instrument performs a transillumination optical scan of the breast.[29] The two laser diodes employed as light sources emit at 685 and 825 nm. The average emitted power is about 10 mW. The laser intensities at 685 and 825 nm are sinusoidally modulated at a frequency of 110.0010 MHz and 110.0008 MHz, respectively. The intensity modulation is obtained by direct modulation of the supplied current provided by a DDS (Direct Digital Synthesizer) frequency synthesizer and radio frequency amplifiers. The optical detector is an avalanche photodiode (APD) (Advanced Photonics, Inc. model SD060-70-62-521). The APD output current is sent to one input of a mixer, and the other mixer input receives a signal at a fre-

quency of 110 MHz. The mixer output contains low frequency components at 1 kHz (relative to the signal at 685 nm) and at 800 Hz (relative to the signal at 825 nm). These two low frequency signals are digitally filtered and processed to yield the frequency-domain raw data (ac amplitude and phase Φ) at both wavelengths. The separation between the signals at 685 and 825 nm is obtained electronically, not optically. The apparatus does not employ optical fibers. The laser beams are collimated by means of aspheric and cylindrical lenses, and dielectrically coated optical prisms make them collinear. The APD detector has a high numerical aperture of approximately 0.4, thus providing highly efficient collection of transmitted light. In a typical measurement, the laser beam and the APD detector are scanned in tandem, thereby continuously maintaining collinearity. The diameter of the laser beam is 2 mm, and the APD's sensitive area is 1.5 mm^2. The breast is compressed between two transparent glass plates and occupies the spatial region between laser diodes and the APD detector (transillumination mode). The entire compression assembly with the two glass plates can be rotated by 90 degrees to allow for data acquisition in craniocaudal and mediolateral projections. The raster scan is performed continuously, line by line, at a speed of about 1 cm/sec. Data acquisition is unidirectional. The pixel size is selected by software. Typically, it is (1-2)mm×(1-2)mm. The acquisition time per data point is about 100 ms, and the time required for a complete breast scan is of the order of 3 minutes.

III. THE PROBLEM OF EDGE EFFECTS

A. Statement of the problem

Transillumination optical scanning produces bidimensional projection images of the breast. In pixels close to the edge of this 2-D image, the measurement's fidelity presents at least two problems:

(1) *Breast thickness variability*. The thickness of breast tissue, that coincides with the separation between the glass plates in the central part of the image, decreases towards the edge of the image;

(2) *Lateral photon losses*. As the scanner approaches the edge of the breast, additional photons are lost through the sides of the breast.

These two problems, that we collectively designate as "edge effects," are pictorially described in Fig. 2. We found that edge effects dominate the raw data images, at least in our sampling geometry. As a result, the presence of optical inhomogeneities, such as a tumor, appear in the optical images as a slight deformation of the general pattern determined by edge effects. Under these conditions, image contrast is strongly reduced, and the sensitivity to tumor detection is weakened.

B. Approach to edge correction

Our approach to the problem of edge effects is based on two observations. We dedicate this section to the description and discussion of these observations.
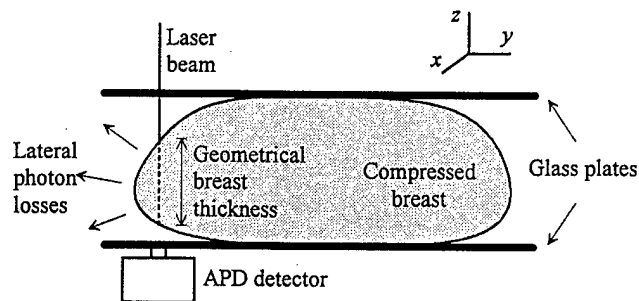
FIG. 2. Pictorial description of edge effects in transillumination optical scanning of the female breast. The geometrical breast thickness along the source-detector line changes during the scan in the x-y plane. When the scanner approaches the edge of the breast, there are additional photon losses through the sides of the breast. Thickness variability and lateral photon losses are collectively indicated as edge effects.

FIG. 3. Dependence of the ac signal at 110 MHz on source-detector separation r for a medium with $\mu_a = 0.03$ cm^{-1} and $\mu_s' = 10$ cm^{-1}. The solid curve refers to the slab geometry, the dashed curve to the $r^{-\alpha}$ decay with $\alpha = 3$. The two curves are normalized at $r = 6$ cm.

Observation 1. The measured phase is linearly dependent on the geometrical breast thickness along the source-detector line, and is not significantly affected by photon losses through the sides of the breast.

The implication of this observation is that breast thickness variability along the scanned region yields the dominant contribution to the measured phase. To understand why this is the case, we should consider the other three main factors that influence the phase reading: (a) photon lateral losses; (b) variability of the optical pathlength in air; (c) effects related to tissue inhomogeneities. A possible way to evaluate the impact of factors (a) and (b) on the measured phase is based on the predictions of diffusion theory. This theoretical model provides an adequate description of light propagation in biological tissue. The basic diffusion equation is:[30]

$$\frac{\partial U}{\partial t} - vD\nabla^2 U + v\mu_a U = q_0,\qquad(1)$$

where U is the photon density, v is the velocity of light in the medium, D is the diffusion coefficient defined as $1/3\mu_s'$ (with μ_s' linear reduced scattering coefficients) (Ref. 31), and q_0 is the isotropic source term. The Green's function of Eq.(1) for the photon flux has been derived for uniform media in a number of geometries, in particular for the infinite slab, sphere, and cylinder.[32] Arridge *et al.* have shown that the frequency-domain phase is almost linearly dependent on the source-detector separation in all three geometries.[32] Furthermore, the differences between the predicted phases in the three geometries are small, implying that the additional photon losses in the spherical and cylindrical geometries do not significantly affect the phase.[32] These results account for the observed linear dependence of Φ on tissue thickness, and for the insensitivity of the phase to lateral photon losses (factor (a)). The variability of tissue thickness along the scanned region is accompanied by a variability in optical pathlength in air. However, this latter effect has little influence on the measured phase. In fact, the phase shift per unit distance traveled in air (1.2° cm^{-1} at 100 MHz modulation frequency) is typically one order of magnitude smaller than the phase shift per unit distance in tissue ($\approx 20°$ cm^{-1} at 100

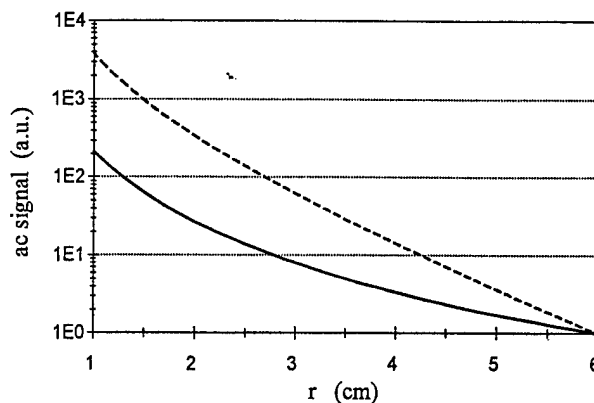MHz modulation frequency) (factor (b)). More importantly, the phase shift in air is also linear with traveled distance, so that the overall linear dependence of phase on tissue thickness is not affected. To evaluate the importance of localized tissue inhomogeneities, one should keep in mind the order of magnitude of a 2–3 cm tissue thickness variation effect, which is of tens of degrees in the phase. The change in phase due to a strong absorber 1 cm in diameter is of the order of 1 degree at modulation frequencies of about 100 MHz (Refs. 33,34,20). This effect (factor (c)) constitutes a slight perturbation to the general phase pattern determined by tissue thickness variations.

Observation 2. The edge effects on the measured ac amplitude can be modeled by a functional dependence on tissue thickness (r) as $r^{-\alpha}$, with $\alpha > 0$.

This result is less rigorous and general than that of observation 1. The attenuation of the ac amplitude with the thickness of an infinite slab is stronger than exponential. We have calculated this attenuation for a medium with $\mu_a = 0.03$ cm^{-1} and $\mu_s' = 10$ cm^{-1} on the basis of the Green's function reported in Ref. 32. The result is shown in Fig. 3 for slab thicknesses ranging from 1 to 6 cm. For comparison, the negative power dependence on thickness (with $\alpha = 3$) is also shown in Fig. 3. Lateral photon losses contribute to the observed reduction in the increase of ac signal at smaller values of r. However, there is also a contribution from the different optical coupling between tissue and both source and detector. As can be seen in Fig. 2, the tissue thickness reduction corresponds to a change in the angle of light incidence and to an increased distance between tissue surface and both source and detector. This fact, together with the non-perfect collimation of laser beam and APD detector, accounts for a variation in source/tissue and tissue/detector optical couplings. We have experimentally verified—on breast simulating phantoms—that this coupling effect is not dominant in our instrument. In our case, the $r^{-\alpha}$ dependence of the ac signal is thus mainly determined by lateral photon losses. Typically, we found α to be in the range 1–3. It is noteworthy that the effect of scattering[35] or absorbing mac-
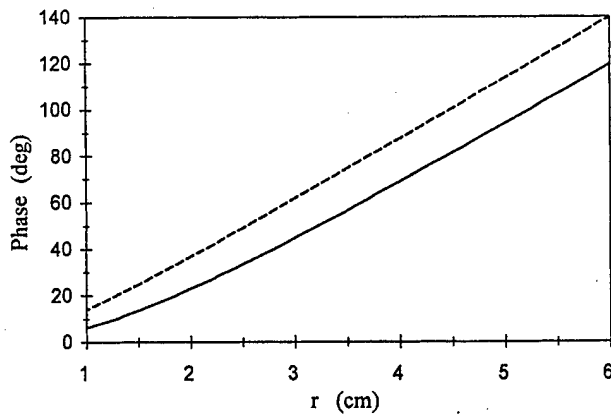
FIG. 4. Comparison between spatial dependence of the phase at 110 MHz in the infinite (dashed line) and slab (solid line) geometries in a medium with $\mu_a = 0.03$ cm^{-1} and $\mu_s' = 10$ cm^{-1}. The spatial coordinate r is the distance between source and detector in the infinite geometry, and the slab thickness in the slab geometry.

roscopic inhomogeneities on the ac amplitude is stronger than that on the phase. For a strong absorber 1 cm in diameter, the ac reduction is about 20–30% (Ref. 33,34,20).

C. Proposed method for edge correction

Let us indicate with x and y the coordinates of a generic pixel in the 2-D projection image. Consequently, we denote with $r(x,y)$ the geometrical thickness at pixel (x,y). On the basis of observation 1 in Section III B, we can write:

$$r(x,y) = r_0 \frac{\Phi(x,y) - \Phi_s}{\Phi_{max} - \Phi_s}, \tag{2}$$

where r_0 is the geometrical separation between the two planes of the compression glass plates (and hence the maximum thickness of the breast), $\Phi(x,y)$ is the phase measured at pixel (x,y), Φ_s is the phase of the source intensity, and Φ_{max} is the maximum measured phase in the scanned region. It is also possible to recover the tissue thickness map $r(x,y)$ from the measured phase without measuring Φ_s. This alternative method is less general because not only does it assume linearity of $\Phi(x,y)$ on $r(x,y)$, but it also assumes a value for the slope $d\Phi(x,y)/dr(x,y)$. The assumed value for the slope is given by:

$$\frac{d\Phi(x,y)}{dr(x,y)} = \left(\frac{\mu_a}{2D}\right)^{1/2} \left\{ \left[1 + \left(\frac{2\pi f}{v\mu_a}\right)^2 \right]^{1/2} - 1 \right\}^{1/2}, \tag{3}$$

where f is the modulation frequency of the source intensity. Equation (3) rigorously describes the spatial dependence of the phase in the infinite geometry.[26,36] However, it is a good approximation for the slab geometry, as is shown in Fig. 4. In Fig. 4, the spatial dependence of the phase in the slab geometry (from Ref. 32) essentially coincides with that in the infinite geometry for source-detector distances over 3 cm. The case reported in Fig. 4 assumes typical values for the optical coefficients of the breast in the near-infrared
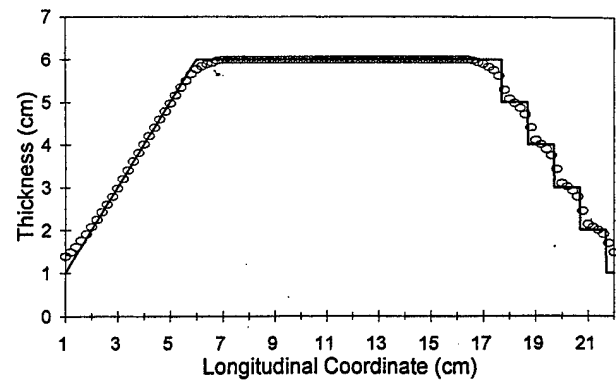

FIG. 5. Actual (solid line) and calculated (symbols) geometrical thickness of the Delrin solid block. The calculation was carried out using Eq. (4) at 685 nm. Similar results were obtained at 825 nm.

($\mu_a = 0.03$ cm^{-1}, $\mu_s' = 10$ cm^{-1}) (Refs. 37,25), and a modulation frequency of 110 MHz. From Eq. (3), the tissue thickness in pixel (x,y) can be written as:

$$r(x,y) = r_0 + \frac{\Phi(x,y) - \Phi_{max}}{\left(\frac{\mu_a}{2D}\right)^{1/2} \left\{ \left[1 + \left(\frac{2\pi f}{v\mu_a}\right)^2 \right]^{1/2} - 1 \right\}^{1/2}}. \tag{4}$$

The required knowledge of Φ_s in Eq. (2) is replaced in Eq. (4) by the required knowledge of the average optical coefficients of the examined tissue μ_a and D.

Once $r(x,y)$ is obtained from either Eq. (2) or Eq. (4), it is possible to derive a calculated parameter, that we call $N(x,y)$, that corrects for edge effects but maintains all the information of the ac signal, relative to optical inhomogeneities. On the basis of observation 2 in Section III B, we define $N(x,y)$ as:

$$N(x,y) = \frac{r_0^\alpha ac_0}{r^\alpha(x,y) ac(x,y)}, \tag{5}$$

where ac_0 is the ac amplitude measured at a specific pixel where breast thickness is r_0, and $ac(x,y)$ is the amplitude measured at pixel (x,y). The value of the parameter α depends on the shape of the examined tissue and on the variations of source/tissue and tissue/detector optical coupling within the scanned region. For our instrument, phantom data were best corrected with $\alpha = 3$ and human breast data were best corrected with $\alpha = 1$. In this paper, we present results obtained using Eq. (4) to calculate $r(x,y)$.

IV. LABORATORY RESULTS

As an initial test, we verified the effectiveness of Eq. (4) in determining the thickness of a sample $r(x,y)$. We employed a solid block of Delrin, a substance that shows weak absorption and strong scattering in the visible/near-infrared spectral region. This Delrin block has a central region 6 cm thick, 11.7 cm long, and 11.4 cm wide. On two sides of the block the thickness decreases, in a smooth way on one side and by

TABLE I. Measured absorption and reduced scattering coefficients of the Delrin block.

λ (nm)	μ_a (cm^{-1})	μ_s' (cm^{-1})
685	0.019 ± 0.001	13.2 ± 0.5
825	0.023 ± 0.001	11.9 ± 0.5

steps on the other. The total length of the block is 23 cm. The side view of the sample is shown in Fig. 5, where we also report the thickness calculated from Eq. (4). To apply Eq. (4) we need to know the average optical coefficients μ_a and μ_s' of the sample. We measured them using the pre-calibrated measurement protocol described elsewhere.[38] The results at the two wavelengths are reported in Table I. These values of μ_a and μ_s' are similar to reported values for breast tissue *in vivo* in the same spectral region.[37,25] The calculated thickness (from the phase at 685 nm) is in excellent agree-

ment with the actual value down to about 1 cm. The deviations from the actual value are always less than 3 mm. The step side of the phantom shows a poorer agreement between calculated r and actual r, but the deviations are still small. Of course, a real breast does not present step variations in thickness. A similar result is obtained from the phase at 825 nm. The Delrin phantom also contains a cylindrical scattering inhomogeneity (about 4 mm in diameter) along its longitudinal symmetry axis. The edge effects problem is well illustrated in Fig. 6(a), where we report the ac raw data image of the Delrin block at 685 nm. The central scattering inhomogeneity is invisible, because the image is dominated by edge effects mainly due to sample thickness variations. In Fig. 6(b) we show an optical image based on the parameter N with $\alpha=3$. Not only are edge effects strongly reduced, but the longitudinal scattering inhomogeneity is now clearly visible. The pixel size is 2 mm×2 mm in both images.
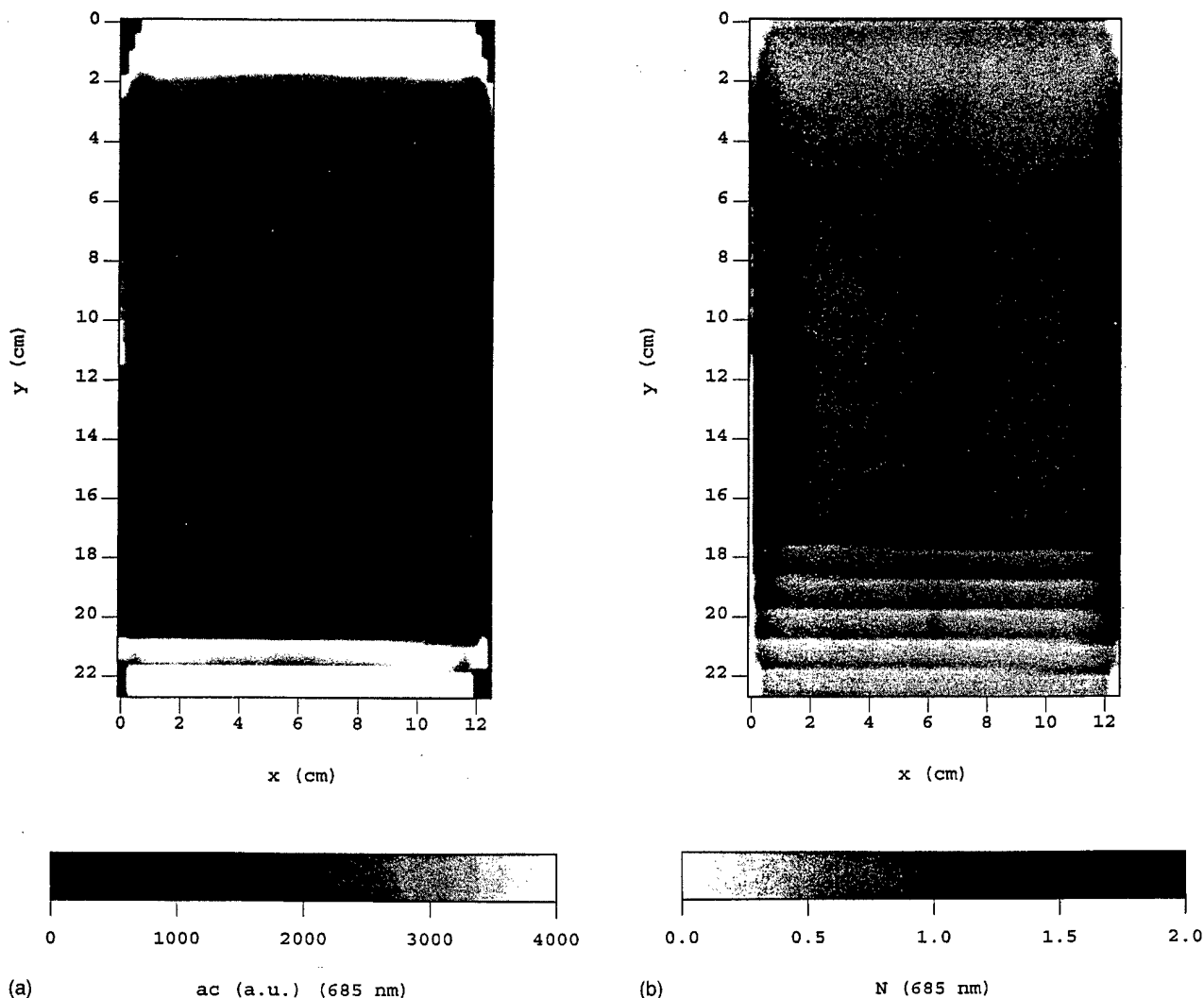

FIG. 6. Optical images of the Delrin solid block at 685 nm. (a) ac image, (b) N image with $\alpha=3$. The average optical coefficients of the sample at this wavelength ($\mu_a=0.019$ cm^{-1}, $\mu_s'=13.2$ cm^{-1}) match those of breast tissue. The sample thickness r varies along the y axis. It increases smoothly from $y=0$ to $y=6$ cm ($r=0$ at $y=0$, $r=6$ cm at $y=6$ cm), then it remains constant ($r=6$ cm) from $y=6$ cm to $y=17.7$ cm, and finally decreases by 1 cm-steps from $y=17.7$ cm to $y=23$ cm. Along the longitudinal axis ($x=6.4$ cm) is located a cylindrical scattering inhomogeneity about 4 mm in diameter.
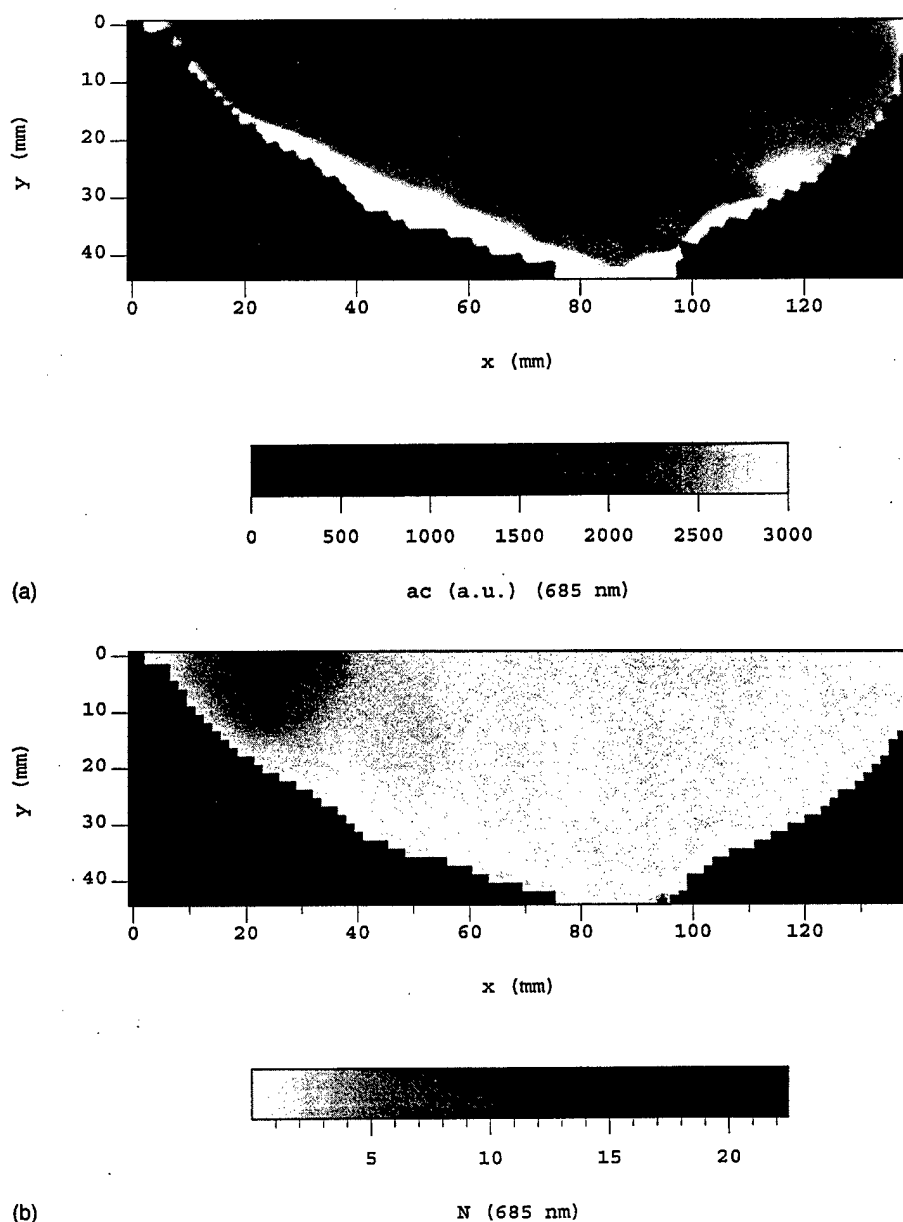
FIG. 7. Optical images at 685 nm in craniocaudal projection of a breast affected by tumor. (a) ac image, (b) N image with $\alpha=1$.

V. CLINICAL RESULTS

To show the effectiveness of our approach in processing optical data from human breasts, we have studied a number of clinical cases. We present here the results for a typical case, with the purpose of pointing out the kind of improvement offered by N images with respect to raw data ac images. A discussion of clinical results goes beyond the purpose of this article, and is presented in a separate paper.[39] To apply Eq. (4) to breast data, we have assumed the following average values of μ_a and μ_s' for breast tissue at λ_1 (685 nm) and λ_2 (825 nm): $\mu_a(\lambda_1)=0.020$ cm^{-1}, $\mu_a(\lambda_2)=0.025$ cm^{-1}, $\mu_s'(\lambda_1)=10$ cm^{-1}, $\mu_s'(\lambda_2)=9$ cm^{-1}. These values are consistent with values reported in the literature.[37,25] Figures 7 and 8 report optical images at 685 nm in craniocaudal and mediolateral projections, respectively. They were taken

on a breast affected by cancer as diagnosed by x-ray mammography and histological examination following needle biopsy. The tumor size is about 1.5 cm. The patient is a 33 year old Caucasian female. Panels (a) of Figs. 7 and 8 are ac images, whereas panels (b) are N images with $\alpha=1$. Pixel size is 1.5 mm$\times$1.5 mm. The edge effects dominate the ac images, and the tumor is not clearly discernible. Image contrast and the effectively imaged area are significantly improved in the N images. An optical inhomogeneity clearly appears in the N images in the tumor region. The gray level distribution is linear in both the ac and N images, but only the N images are full scale (white corresponds to the smallest value, black to the highest). In the ac images a scale reduction was necessary to enhance their features in the central region of the breast.
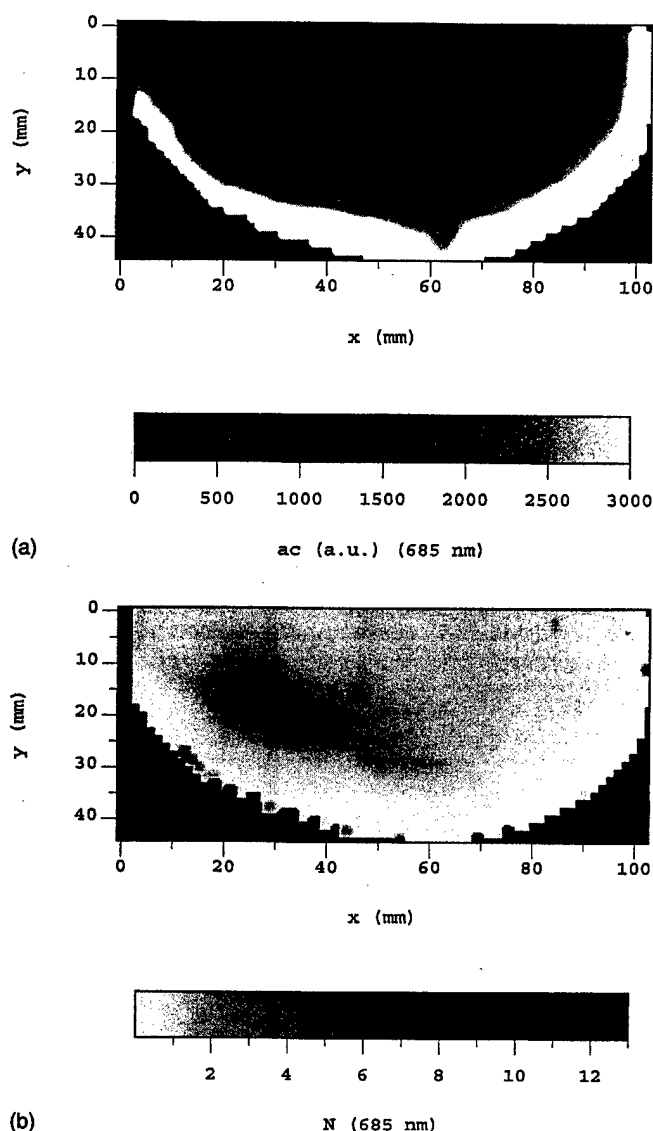
FIG. 8. Optical images at 685 nm in mediolateral projection of the same breast shown in Fig. 7. (a) ac image, (b) N image with $\alpha=1$.

VI. DISCUSSION

A. Use of ac signal information

Our method uses the phase information to obtain the tissue thickness map $r(x,y)$. The knowledge of $r(x,y)$ is then used to improve contrast and detectability in the ac image. This approach enhances features present in the ac image without adding phase information of optical inhomogeneities. The most important consequence of this procedure is that the N image provides only qualitative information about tumor size. The fact that the ac image pattern is insensitive to the size of small optical inhomogeneities (below 1 cm in linear size) was shown experimentally.[33] For this reason, our N image can be considered useful as a detection tool, but it has limited spatial diagnostic significance. As stated in the introduction, our approach is aimed at improving contrast and detectability, rather than resolution and size evaluation. Another consequence of using only ac information to detect

optical defects is that we are not capable of recognizing scattering from absorbing inhomogeneites. As of today, it is not clear whether tumors behave as stronger absorbers or stronger scatterers than healthy tissue. However, a separation between absorption and scattering effects may yet result in an effective way of achieving specificity.

B. Use of single wavelength data

The parameter $N(x,y)$ is obtained from single wavelength data. The detection of a tumor is thus based on the difference between its optical properties and those of healthy tissue at that wavelength. It is possible to correct for edge effects also by employing data at two different wavelengths. In this case, the idea is that the raw data (phase and ac) are influenced by edge effects to the same extent at the two wavelengths. This is a reasonable assumption. By following this two-wavelength method, we were able to correct very well for edge effects. The drawback of the two-wavelength approach is that the tumor's detectability is based on the different spectral dependence of the tumor's optical properties and those of healthy tissue between those two wavelengths. The choice of the two wavelengths thus becomes critical. It may also be dictated by the particular kind of tumor and/or biological tissue. The use of multiple wavelengths could still be a valuable tool, and is actually being thoroughly investigated.[40,41] In our experience to date, the two-wavelength method at 685 and 825 nm was often successful in tumor detection, but contrast and detectability were improved by the single wavelength $N(x,y)$ map.

C. Significance of the absolute value of the parameter $N(x,y)$

Since r_0 and ac_0 are constants, contrast and detectability of the N image would not be affected by their absence in the definition of Eq. (5). They simply introduce a scale factor in the N map. However, we include them in the definition of N to study the information content of the absolute value of N. In the absence of inhomogeneities, the N image ideally assumes a constant value of 1. In reality, the image is not totally flat because of intrinsic tissue inhomogeneities and imperfect correction of edge effects. An absorbing or scattering defect causes a decrease in $ac(x,y)$ and hence a value of $N(x,y)$ greater than 1. We found a good correlation between the presence of tumors and values of $N(x,y)$ greater than 2. Even if we are not aiming at specificity, it might be possible that a value of N higher than 2 constitutes a sufficient (but not necessary) condition for the presence of a tumor. We are currently investigating the diagnostic significance of the absolute value of $N(x,y)$ in a larger number of clinical cases.

D. Estimate of the optical coefficients of breast tissue

In Section III C we have presented two ways to obtain $r(x,y)$ from the measured phase. The first one (Eq. (2)) requires a measurement of the source intensity phase Φ_s. The second one (Eq. (4)) requires a measurement or an estimate of the average value of μ_a and μ_s' of breast tissue. In this

article, we have followed the second approach based on Eq. (4). In applying Eq. (4) to breast data, we have used values for μ_a and μ_s' of breast tissue reported in the literature.[37,25] Even if these studies report a small variability of the optical coefficients among individuals, a question may arise as to how critical is the choice of these values? In other words, how much is the calculated thickness affected by a misjudged estimate of μ_a and/or μ_s'? To a first approximation, even if the estimated values of μ_a and μ_s' are off by as much as 50%, the maximum deviation between real and calculated r is less than 1 cm. However, this deviation constitutes a systematic error that will not significantly affect the contrast of the $N(x,y)$ image. The use of Eq. (2) will remove this source of error, provided that the measurement of Φ_s can be performed with appropriate accuracy.

VII. CONCLUSION

In this paper, we have investigated the problem of edge effects in the laser-beam transillumination scan of the human breast. Our results show that edge effects can be effectively corrected in the frequency-domain, yielding high contrast images and excellent detectability. Furthermore, the corrected images do not require any adjustment of scale amplitude or gray level distribution. The optical images can thus be displayed during the clinical exam in real time with no additional manipulations. Our results show practical feasibility of frequency-domain optical mammography. We are currently investigating the clinical value of such an optical tool by carrying out a systematic analysis of optical mammography results in a number of clinical cases.

ACKNOWLEDGMENTS

[1]M. Cutler, "Transillumination of the Breast," Surg. Gynecol. Obstet. **48**, 721–727 (1929).

[2]C. M. Gros, Y. Quenneville, and Y. Hummel, "Diaphanologie Mammaire," J. Radiol. Electrol. Med. Nucl. **53**, 297–306 (1972).

[3]B. Ohlsson, J. Gundersen, and D. M. Nilsson, "Diaphanography: A Method for Evaluation of the Female Breast," World J. Surg. **4**, 701–706 (1980).

[4]E. Carlsen, "Transillumination Light Scanning," Diagn. Imaging **4**, 28–34 (1982).

[5]V. Marshall, D. C. Williams, and K. D. Smith, "Diaphanography as a Means of Detecting Breast Cancer," Radiology **150**, 339–343 (1984).

[6]B. Drexler, J. L. Davis, and G. Schofield, "Diaphanography in the Diagnosis of Breast Cancer," Radiology **157**, 41–44 (1985).

[7]A. Alveryd, I. Andersson, K. Aspegren, G. Balldin, N. Bjurstam, G. Edström, G. Fagerberg, U. Glas, O. Jarlman, S. A. Larsson, E. Lidbrink, H. Lingaas, M. Löfgren, C.-M. Rudenstam, L. Strender, L. Samuelsson, L. Tabàr, A. Taube, H. Wallberg, P. Akesson, and D. Hallberg, "Lightscanning Versus Mammography for the Detection of Breast Cancer in Screening and Clinical Practice," Cancer **65**, 1671–1677 (1990).

[8]G. A. Navarro and E. Profio, "Contrast in the Diaphanography of the Breast," Med. Phys. **15**, 181–187 (1988).

[9]A. H. Gandjbakhche, R. Nossal, and R. F. Bonner, "Resolution Limits for Optical Transillumination of Abnormalities Deeply Embedded in Tissues," Med. Phys. **21**, 185–191 (1994).

[10]G. Jarry, S. Ghesquiere, J. M. Maarek, F. Fraysse, S. Debray, B. M. Hung, and D. Laurent, "Imaging Mammalian Tissues and Organs Using Laser Collimated Transillumination," J. Biomed. Eng. **6**, 70–74 (1984).

[11]Y. Yamashita and M. Kaneko, "Visible and Infrared Diaphanoscopy for Medical Diagnosis," in *Medical Optical Tomography: Functional Imaging and Monitoring*, edited by G. J. Muller *et al.* (SPIE, Bellingham, WA, 1993), pp. 283–316.

[12]D. Jarlman, "Diagnostic Transillumination of the Breast," Ph.D. thesis, Lund University, Lund, Sweden (1991).

[13]D. T. Delpy, M. Cope, P. van der Zee, S. Arridge, S. Wray, and J. Wyatt, "Estimation of Optical Pathlength through Tissue from Direct Time of Flight Measurement," Phys. Med. Biol. **33**, 1433–1442 (1988).

[14]M. S. Patterson, B. Chance, and B. C. Wilson, "Time Resolved Reflectance and Transmittance for the Non-Invasive Measurement of Optical Properties," Appl. Opt. **28**, 2331–2336 (1989).

[15]E. Gratton, W. W. Mantulin, M. J. vande Ven, J. B. Fishkin, M. B. Maris, and B. Chance, "The Possibility of a Near-Infrared Optical Imaging System Using Frequency-Domain Methods," *Third International Conference for Peace through Mind/Brain Science*, 5–10 August 1990, Hamamatsu City (Hamamatsu Photonics K. K., Hamamatsu City, Japan, 1990), pp. 183–189.

[16]B. Chance, M. Maris, J. Sorge, and M. Z. Zhang, "A Phase Modulation System for Dual Wavelength Difference Spectroscopy of Haemoglobin Deoxigenation in Tissue," Proc. SPIE **1204**, 481–491 (1990).

[17]B. J. Tromberg, L. O. Svaasand, T. T. Tsay, R. C. Haskell, and M. W. Berns, "Optical Property Measurement in Turbid Media Using Frequency-Domain Photon Migration," Proc. SPIE **1525**, 52–58 (1991).

[18]E. M. Sevick, J. Weng, M. Maris, and B. Chance, "Analysis of Absorption, Scattering, and Hemoglobin Saturation Using Phase Modulation Spectroscopy," Proc. SPIE **1431**, 264–275 (1991).

[19]M. S. Patterson, J. D. Moulton, B. C. Wilson, K. W. Berndt, and J. R. Lakowicz, "Frequency-Domain Reflectance for the Determination of the Scattering and Absorption Properties of Tissue," Appl. Opt. **30**, 4474–4476 (1991).

[20]J.-M. Kaltenbach and M. Kaschke, "Frequency- and Time-Domain Modelling of Light Transport in Random Media," in *Medical Optical Tomography: Functional Imaging and Monitoring*, edited by G. J. Muller *et al.* (SPIE, Bellingham, WA, 1993), pp. 65–86.

[21]J. C. Hebden and R. A. Kruger, "Transillumination Imaging Performance: Spatial Resolution Simulation Studies," Med. Phys. **17**, 41–47 (1990).

[22]L. Wang, P. P. Ho, C. Liu, G. Zhang, and R. R. Alfano, "Ballistic 2-D Imaging Through Scattering Walls Using an Ultrafast Optical Kerr Gate," Science **253**, 769–771 (1991).

[23]D. A. Benaron and D. K. Stevenson, "Optical Time-of-Flight and Absorbance Imaging of Biologic Media," Science **259**, 1463–1466 (1993).

[24]S. R. Andersson-Engels, R. Berg, S. Svanberg, and O. Jarlman, "Time Resolved Transillumination for Medical Diagnostic," Opt. Lett. **15**, 1179–1181 (1990).

[25]G. Mitic, J. Kölzer, J. Otto, E. Plies, G. Sölkner, and W. Zinth, "Time-Gated Transillumination of Biological Tissues and Tissuelike Phantoms," Appl. Opt. **33**, 6699–6710 (1994).

[26]J. B. Fishkin and E. Gratton, "Propagation of Photon-Density Waves in Strongly Scattering Media Containing an Absorbing SemiInfinite Plane Bounded by a Straight Edge," J. Opt. Soc. Am. A **10**, 127–140 (1993).

[27]P. Krämmer, H. Bartelt, H. Fischer, and B. Schmauss, "Imaging in Scattering Media Using the Phase of Modulated Light Sources," Proc. SPIE **2326**, 65–74 (1995).

[28]S. Fantini, M. A. Franceschini, J. B. Fishkin, B. Barbieri, and E. Gratton, "Quantitative Determination of the Absorption Spectra of Chromophores in Strongly Scattering Media: a Light-EmittingDiode Based Technique," Appl. Opt. **33**, 5204–5213 (1994).

[29]M. Kaschke, H. Jess, G. Gaida, J. M. Kaltenbach, and W. Wrobel, "Transillumination Imaging of Tissue by Phase Modulation Techniques," in *Advances in Optical Imaging and Photon Migration*, edited by R. R. Alfano, Proc. OSA **21**, 88–92 (1994).

[30]J. J. Duderstadt and L. J. Hamilton, *Nuclear Reactor Analysis* (Wiley, New York, 1976).

[31]K. Furutsu and Y. Yamada, "Diffusion Approximation for a Dissipative Random Medium and the Applications," Phys. Rev. E **50**, 3634–3640 (1994).

[32]S. R. Arridge, M. Cope, and D. T. Delpy, "The Theoretical Basis for the Determination of Optical Pathlengths in Tissue: Temporal and Frequency Analysis," Phys. Med. Biol. **37**, 1531–1560 (1992).

[33]E. Gratton and J. Maier, "Frequency-Domain measurement of Photon Migration in Highly Scattering Media," in *Medical Optical Tomography: Functional Imaging and Monitoring*, edited by G. J. Muller *et al.* (SPIE, Bellingham, WA, 1993), pp. 534–544.

[34]A. H. Hielscher, F. K. Tittel, and S. L. Jacques, "Imaging in Biological Tissues by Means of Diffraction Tomography with Photon Density Waves," Proc. SPIE **2326**, 75–85 (1995).

[35]D. G. Papaioannou, S. B. Colak, and G. W. Hooft, "Resolution and Sensitivity Limits of Optical Imgaing in Highly Scattering Media," Proc. SPIE (in press).

[36]S. Fantini, M. A. Franceschini, and E. Gratton, "Semi-Infinite Geometry Boundary Problem for Light Migration in Highly Scattering Media: A Frequency-Domain Study in the Diffusion Approximation," J. Opt. Soc. Am. B **11**, 2128–2138 (1994).

[37]K. A. Kang, B. Chance, S. Zhao, S. Srinivasan, E. Patterson, and R. Troupin, "Breast Tumor Characterization Using Near-Infra-Red Spectroscopy," Proc. SPIE **1888**, 487–499 (1993).

[38]M. A. Franceschini, S. Fantini, S. A. Walker, J. S. Maier, and E. Gratton, "Multi-Channel Optical Instrument for Near-Infrared Imaging of Tissue," Proc. SPIE **2389**, 264–272 (1995).

[39]M. A. Franceschini, K. T. Moesta, S. Fantini, G. Gaida, E. Gratton, H. Jess, W. W. Mantulin, M. Seeber, P. M. Schlag, and M. Kaschke, "Frequency-Domain Instrumentation Enhances Optical Mammography: Initial Clinical Results," submitted to Nature Med.

[40]S. Ertefai and A. E. Profio, "Spectral Transmittance and Contrast in Breast Diaphanography," Med. Phys. **12**, 393–400 (1985).

[41]H. Heusmann, J. Kölzer, J. Otto, R. Puls, T. Friedrich, S. Heywang-Köbrunner, and W. Zinth, "Spectral Transillumination of Female Breasts and Breast Tissue-Like Material," Proc. SPIE **2326**, 370–382 (1995).

Optical Mammography with Intensity-Modulated Light

Sergio Fantini, Erica L. Heffer, Maria Angela Franceschini
Bioengineering Center, Department of Electrical Engineering and Computer Science,
Tufts University, 4 Colby Street, Medford, MA 02155, USA
sergio.fantini@tufts.edu

Linda Götz, Anke Heinig, Sylvia Heywang-Köbrunner
Martin Luther Universitaet Halle/Wittenberg, Institut für Diagnostische Radiologie und CT
Magdeburgerstraße 16, D-06097 Halle, Germany

Oliver Schütz, Horst Siebold
Siemens AG, Medical Engineering, Postfach 3260, 91050 Erlangen, Germany

Abstract: We report the results of our initial analysis of the frequency-domain optical mammograms collected on a clinical population of 131 patients. The instrument for optical mammography employs four intensity-modulated (at 70 MHz) laser diodes emitting at 690, 750, 788, and 856 nm. The amplitude and phase images of the breast are combined to produce edge-corrected optical images at each of the four wavelengths. The one-wavelength (690 nm) edge-corrected images have been examined according to two different criteria for the assignment of positive optical mammograms. Criterion 1 requires both views of the breast to be positive, while criterion 2 requires at least one view to be positive. The resulting (sensitivity; specificity) was (72%; 52%) (criterion 1) and (88%; 30%) (criterion 2). We show how adding spectral information can improve on these results.
OCIS codes: (170.0170) Medical optics and biotechnology; (110.0110) Imaging systems; (170.4580) Optical diagnostics for medicine; (170.3830) Mammography; (110.7050) Turbid media

1. Introduction

Optical mammography is a safe, painless, and cost-effective technique that may become a useful clinical tool for the detection and diagnosis of breast cancer. It employs near-infrared light (typically in the wavelength range 670-970 nm) to non-invasively probe the female breast. Over this spectral region, hemoglobin is the dominant intrinsic contrast agent. The hemoglobin concentration and its oxygen saturation are two key parameters that may allow not only the detection of cancer, but also the discrimination between malignant and benign breast lesions using optical methods. Optical mammography can be performed using continuous wave (CW) light [1,2], or using time-resolved techniques in the time-domain [3-5] and in the frequency-domain [6-11]. Previous implementations of CW optical mammography in the 1970's and 1980's under the names of diaphanography [12] and lightscanning [13] failed to produce a viable clinical tool because of their inferior performance compared to x-ray mammography [14-18]. In the past decade, the use of diffusion theory to model light propagation into breast tissue, and the introduction of time-resolved optical methods have opened new possibilities in the area of optical mammography. Here, we present our approach to frequency-domain optical mammography, and we report the results of a preliminary analysis of the optical breast images collected on a clinical population of 131 patients.

2. Methods

The block diagram of the apparatus for frequency-domain optical mammography is shown in Fig. 1. This instrument is a four-wavelength, homodyne-in-quadrature system. The four wavelengths (690, 750, 788, 856 nm) are electronically discriminated by modulating the corresponding laser diodes at different frequencies ranging from 69.50 to 70.45 MHz. The modulation is achieved by superimposing a radio-frequency signal to the DC current supplies by means of bias tees. A modulation frequency in the order of 70 MHz is chosen to achieve a phase shift per unit distance of about 20°/cm in breast tissue. A pilot laser at 1310 nm, modulated at 500 kHz, is used to probe the geometrical shape of the breast and to drive protection switches that prevent the photomultiplier tube detector from being overexposed. The emission of the five laser diodes is guided by optical fibers (core diameter: 100 μm) to a fiber coupler. The output of the coupler is an optical fiber having an internal diameter of 400 μm. The numerical aperture of this fiber results in an illuminated area larger than 1 mm^2 on the breast surface. The maximum optical power emitted by the laser diodes at 690, 750, 788, 856, and 1310 nm is 30, 10, 40, 50, and 5 mW, respectively. About 70% of this optical power reaches the skin of the breast via the fiber optics. The maximum irradiance on the skin is therefore 0.7×135 mW/mm^2. This irradiance is kept on a given spot by no longer than the pixel residence time (8 ms) determined by the x-y translational stage. Consequently, the maximum radiant exposure on the skin is 756 mW-ms/mm^2 = 75.6 mJ/cm^2, which is significantly less than the maximum permissible exposure to a laser beam for skin (329 mJ/cm^2) reported by the American National Standard for the safe use of lasers under these conditions [19].
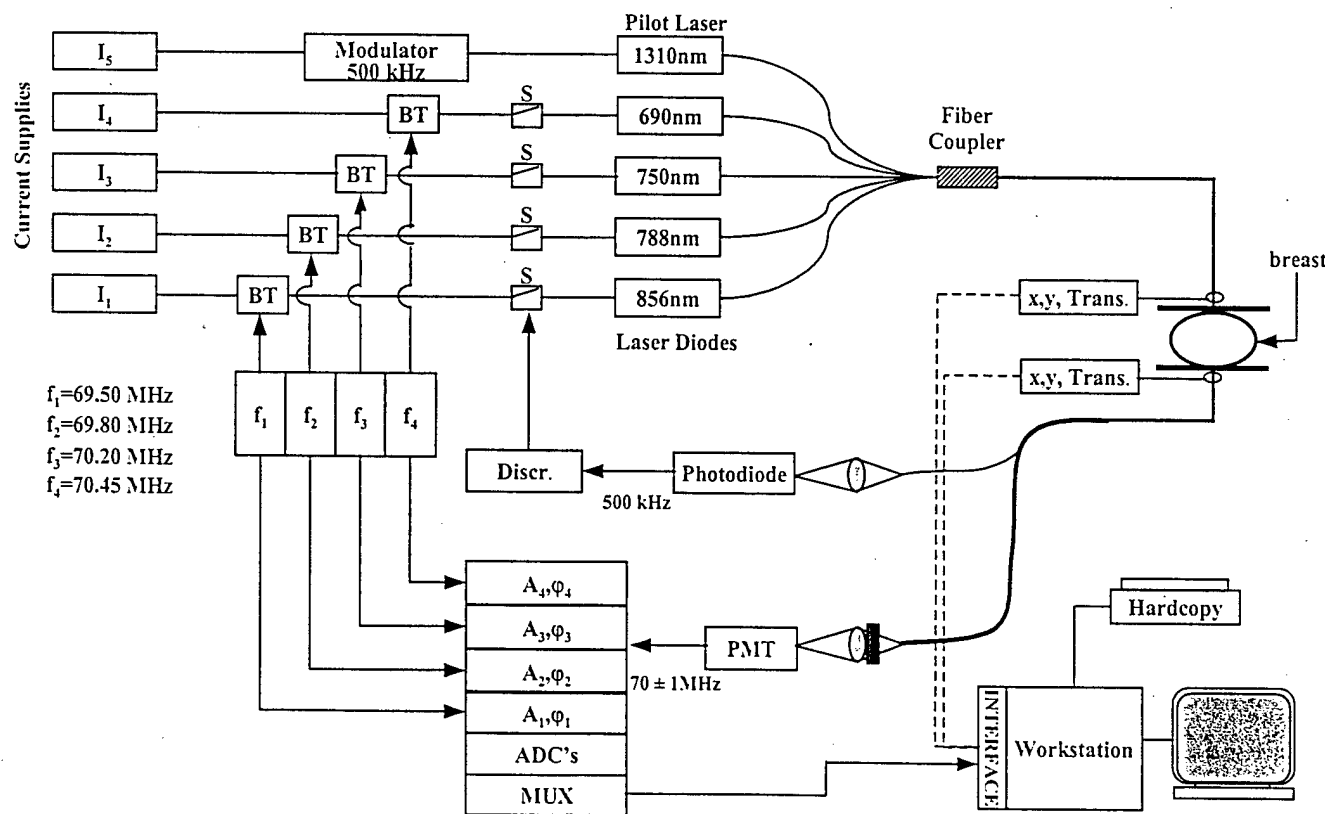

Fig. 1. Block diagram of the instrument for frequency-domain optical mammography. I: current; f: frequency; A: amplitude, φ: phase; BT: bias tee; S: shutter; Discr.: discriminator; x,y Trans.: x,y translational stage; PMT: photomultiplier tube; ADC: analog to digital converter; MUX: multiplexer.

The optical signal is collected in a transmission geometry by an optical fiber bundle having an internal diameter of 5 mm (core diameter of the individual fibers: 60 µm). The source and the detector fibers are located on opposite sides of the breast. About 90% of the collected optical signal is guided to a photomultiplier tube detector (for the 690, 750, 788, and 856 nm signals), and about 10% to a photodiode (for the 1310 nm pilot signal). The instrumental noise measured on a tissue-like phantom without x-y translational motion and with an acquisition time of 8 ms is 0.15% for the amplitude, and 0.1° for the phase. Mechanical scanning increases the instrumental noise. Typical noise levels recorded in a human breast examination (with translational motion, acquisition time per pixel: 8 ms, breast thickness: 4-8 cm) are 2-3% for the amplitude, and 0.5-0.8° for the phase.

During an examination, the breast is slightly compressed between two glass plates. The distance between the compressing plates is measured and recorded during each exam. The optical image of the breast is acquired by performing a continuous tandem scan of the source and detector fibers over the x-y plane defined by the compression plates. The source and detector fibers remain collinear while the scan is being performed. The resulting 2-dimensional projection image of the breast is made of 2×2 mm^2 pixels. The breast compression assembly can be rotated to allow the acquisition of breast images in the craniocaudal and oblique views, as routinely done also in x-ray mammography. The acquisition time required to image the whole breast is about 2 min per view.

The amplitude and phase data are combined into a dimensionless parameter, that we called N, which is related to the optical absorbance of breast tissue [20]. The images based on this parameter (N-images) accomplish a significant correction of edge effects, which are determined by the reduction in breast thickness and by the modified boundary conditions at pixels close to the edge of the breast [20]. As a result, the dynamic range of the N-images is significantly less than that of the amplitude and phase images, and optical inhomogeneities in the breast appear with a higher contrast. Furthermore, N-images are displayed using a linear gray scale over the full range of data in the image (white represents the lowest value, black the highest). This allows for the display of the optical images of the breast in real-time, on-line, during the examination. The examiner is not required to perform any further manipulations to the N-images after acquisition.

We have examined with frequency-domain optical mammography a clinical population of 131 patients. The diagnosis of the cases was determined either by fine needle biopsy or by pathology examination following surgery. In the interpretation of the optical mammograms, we have followed two distinct criteria. The first one (criterion 1), previously reported [21], considers an optical mammogram to be positive if it shows optical abnormalities that are spatially consistent in the two views and that are not thread like. The second one (criterion 2) requires an optical mammogram to show a suspicious region in at least one view to classify the case as a positive finding.

3. Results

The appearance of breast cancer in an optical mammogram is illustrated in Fig. 2. This figure reports the craniocaudal and oblique views, at 690 nm, of the left breast of a 72 year old patient affected by invasive ductal carcinoma. The cancer size is 2.5 cm. Despite the intrinsically low-resolution of optical mammography, the optical image shows this 2.5 cm-diameter cancer with high contrast. The optical contrast is mainly determined by an increased hemoglobin concentration around the cancerous tissue, which significantly increases the local absorption coefficient. The absorption coefficient of cancerous breast tissue can be 2-3 larger than the absorption coefficient of healthy breast tissue [22,23]. Because blood not only absorbs light, but it also scatters it, the smaller scattering contrast observed in breast cancers (factor 1-1.3) [22,23] may also result from the increased blood concentration in the cancerous area. We observe that the N-images are not able to discriminate absorption from scattering contrast.

The dark areas in the two images of Fig. 2 represent areas of higher optical absorbance, but they do not provide information on the relative absorption and scattering contributions to the increased absorbance.

We have examined the one-wavelength (690 nm) N-images from the clinical population according to the two different criteria described in section 2. The results according to criteria 1 and 2 are reported in Table 1.
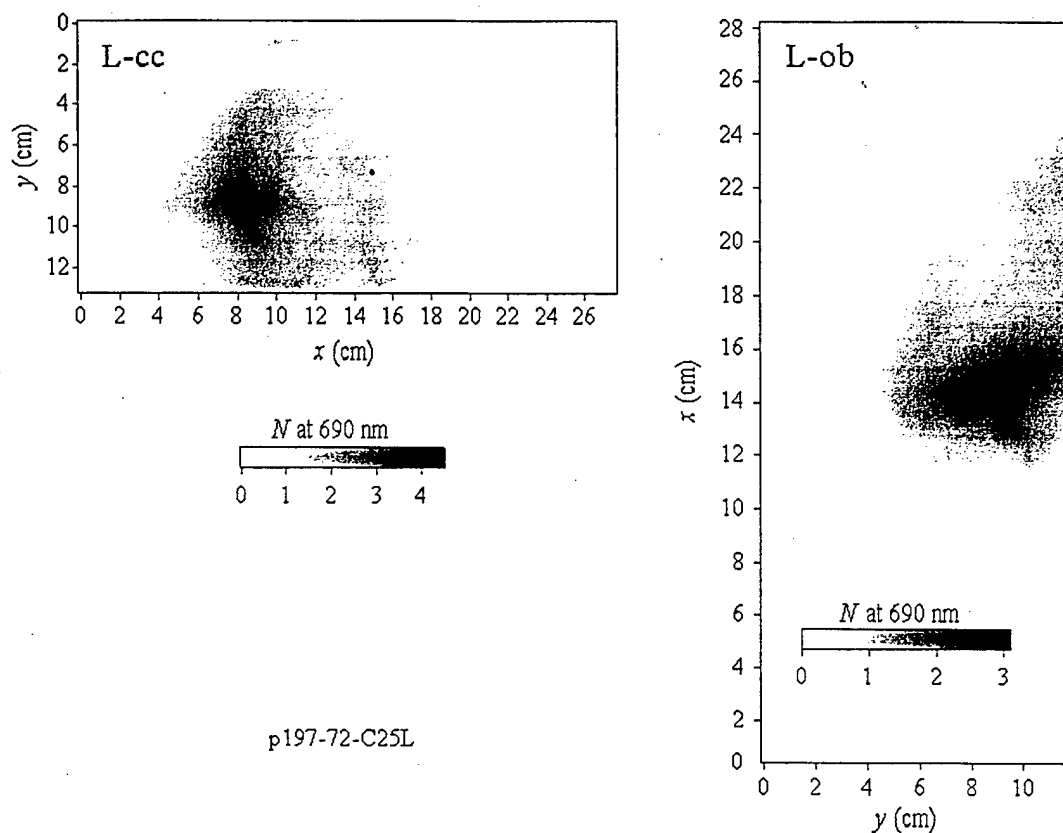

Fig. 2. Craniocaudal (cc) and oblique (ob) views of the left (L) breast of a 72 year old patient affected by invasive ductal carcinoma. Cancer size is 2.5 cm. The cancer appear with high contrast in both views of the breast.

Table 1. Results of the analysis of the 690 nm frequency-domain optical mammograms from a clinical population of 131 patients according to criteria 1 and 2.

	Both views requirement (Criterion 1)	At least one view requirement (Criterion 2)
True positive results (TP)	42	53
True negative results (TN)	79	52
False positive results (FP)	73	122
False negative results (FN)	16	7
Sensitivity: TP/(TP+FN)	72%	88%
Specificity: TN/(TN+FP)	52%	30%
Pos. predictive value: TP/(TP+FP)	37%	30%
Neg. predictive value: TN/(TN+FN)	83%	88%
Test efficiency: (TP+TN)/Total results	58%	44%

The results of Table 1 are based on the *N*-images at one wavelength (690 nm). Additional information can be obtained by considering the images at the other three wavelengths (750, 788, and 856 nm). The specificity of the examination, and therefore the diagnosis potential, can benefit from the analysis of the spectral dependence of the detected breast lesions. For example, Fig. 3 reports the spectral dependences of three different optical inhomogeneities observed in three cases: (1) blood vessel, (2) cancer, and (3) mastopathy. The corresponding optical mammograms (at 690 nm, craniocaudal view) are illustrated on the right hand side of Fig. 3. In Fig. 3, one can observe that spectral features provide a discriminating capability that adds to the morphological information provided by single-wavelength *N*-images.
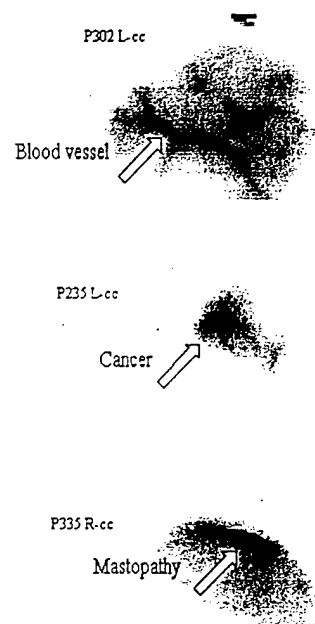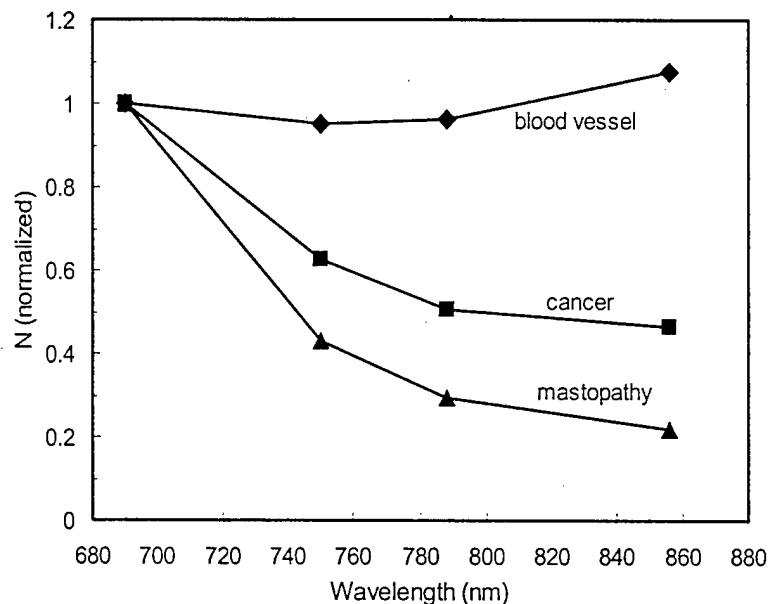

Fig. 3. Spectral discrimination of three structures (a blood vessel, a malignant tumor, and a mastopathy) observed in three optical mammograms.

4. Discussion and Conclusion

The results reported in Table 1 must be interpreted by considering that they are obtained from the analysis of one-wavelength *N*-images, which do not take full advantage of the potential of frequency-domain optical mammography. The characterization of the tumor optical properties, possibly by reconstructing the absorption and scattering images of the breast [9], and the analysis of spectral features, which may give indications on the oxygenation of breast lesions [8], are key factors in optical mammography. By fully exploiting these unique features, it may be possible to improve the performance of optical mammography to a level that renders it a clinically attractive technique.

References

1. Y. Yamashita and M. Kaneko, "Visible and Infrared Diaphanoscopy for Medical Diagnosis," in *Medical Optical Tomography: Functional Imaging and Monitoring*, Editors G. J. Muller et al., (SPIE, Bellingham, Washington, 1993), pp. 283-316.
2. J. H. Hoogenraad, M. B. van der Mark, S. B. Colak, G. W.'t Hooft, and E. S. van der Linden, "First Results from the Philips Optical Mammoscope," in *Photon Propagation in Tissues III*, D. Benaron, B. Chance, and M. Ferrari, eds., Proc. SPIE **3194**, 184-190 (1998).
3. K. Wells, J. C. Hebden, F. E. W. Schmidt, and D. T. Delpy, "The UCL Multichannel Time-Resolved System for Optical Tomography," Proc. SPIE **2979**, 599-607 (1997).
4. D. Grosenick, H. Wabnitz, and H. Rinneberg, "Time-Resolved Imaging of Solid Phantoms for Optical Mammography," Appl. Opt. **36**, 221-231 (1997).
5. R. Cubeddu, A. Pifferi, P. Taroni, A. Torricelli, and G. Valentini, "Noninvasive Absorption and Scattering Spectroscopy of Bulk Diffusive Media: An Application to the Optical Characterization of Human Breast," Appl. Phys. Lett. **74**, 874-876 (1999).
6. M. A. Franceschini, K. T. Moesta, S. Fantini, G. Gaida, E. Gratton, H. Jess, W. W. Mantulin, M. Seeber, P. M. Schlag, and M. Kaschke, "Frequency-Domain Techniques Enhance Optical Mammography: Initial Clinical Results," Proc. Natl. Acad. Sci. USA **94**, 6468-6473 (1997).
7. B. J. Tromberg, O. Coquoz, J. B. Fishkin, T. Pham, E. R. Anderson, J. Butler, M. Cahn, J. D. Gross, V. Venugopalan, and D. Pham, "Non-Invasive Measurements of Breast Tissue Optical Properties Using Frequency-Domain Photon Migration," Phil. Trans. R. Soc. Lond. B **352**, 661-668 (1997).
8. S. Zhou, C. Xie, S. Nioka, H. Liu, Y. Zhang, and B. Chance, "Phased Array Instrumentation Appropriate to High Precision Detection and Localization of Breast Tumor," in *Optical Tomography and Spectroscopy of Tissue: Theory, Instrumentation, Model, and Human Studies II*, B. Chance and R. R. Alfano, eds., Proc. SPIE **2979**, 98-106 (1997).
9. B. W. Pogue, M. Testorf, T. McBride, U. Osterberg, and K. Paulsen, "Instrumentation and Design of a Frequency-Domain Diffuse Optical Tomography Imager for Breast Cancer Detection," Opt. Expr. **1**, 391-403 (1997).
10. X. D. Li, T. Durduran, A. G. Yodh, B. Chance, and D. N. Pattanayak "Diffraction tomography for biochemical imaging with diffuse-photon density waves," Opt. Lett. **22**, 573-575 (1997).
11. K. T. Moesta, S. Fantini, H. Jess, S. Totkas, M. A. Franceschini, M. Kaschke, and P. M. Schlag, "Contrast Features of Breast Cancer in Frequency-Domain Laser Scanning Mammography," J. Biomed. Opt. **3**, 129-136 (1998).
12. C. M. Gros, Y. Quenneville, Y. Hummel, "Diaphanologie Mammaire," J. Radiol. Electrol. Med. Nucl. **53**, 297-306 (1972).
13. E. Carlsen, "Transillumination Light Scanning," Diagn. Imaging **4**, 28-34 (1982).
14. E. A. Sickles, "Breast Cancer Detection with Transillumination and Mammography," AJR **142**, 841-844 (1984).
15. G. E. Geslien, J. R. Fisher, and C. DeLaney, "Transillumination in Breast Cancer Detection: Screening Failures and Potential," AJR **144**, 619-622 (1985).
16. B. Drexler, J. L. Davis, and G. Schofield, "Diaphanography in the Diagnosis of Breast Cancer," Radiology **157**, 41-44 (1985).
17. J. J. Gisvold, L. R. Brown, R. G. Swee, D. J. Raygor, N. Dickerson, and M. K. Ranfranz, "Comparison of Mammography and Transillumination Light Scanning in the Detection of Breast lesions," AJR **147**, 191-194 (1986).
18. A. Alveryd *et al.*, "Lightscanning Versus Mammography for the Detection of Breast Cancer in Screening and Clinical Practice," Cancer **65**, 1671-1677 (1990).
19. American National Standard for the Safe Use of Lasers, ANSI Z136.1-1993 (The Laser Institute of America, Orlando, FL, 1993), Tables 6 and 7.

20. S. Fantini, M. A. Franceschini, G. Gaida, E. Gratton, H. Jess, W. W. Mantulin, K. T. Moesta, P. M. Schlag, and M. Kaschke, "Frequency-Domain Optical Mammography: Edge Effect Corrections," Med. Phys. **23**, 149-157 (1996).

21. S. Fantini, O. Schütz, J. Edler, S. Heywang-Köbrunner, L. Götz, M. A. Franceschini, and H. Siebold, "Clinical Applications of Frequency-Domain Optical Mammography," Proc. SPIE **3566**, 194-199 (1999).

22. S. Fantini, S. A. Walker, M. A. Franceschini, M. Kaschke, P. M. Schlag, and K. T. Moesta, "Assessment of the Size, Position, and Optical Properties of Breast Tumors *in Vivo* by Non-Invasive Optical Methods," Appl. Opt. **37**, 1982-1989 (1998).

23. D. Grosenick, H. Wabnitz, H. H. Rinneberg, K. T. Moesta, and P. M. Schlag, "Development of a Time-Domain Optical Mammograph and First *in vivo* Applications," Appl. Opt. **38**, 2927-2943 (1999).

TOPS Volume 38

Series Editor: Tingye Li

Biomedical

Topical

Meetings

Technical Digest

Postconference Edition

April 2–5, 2000

Fountainbleau Hilton Resort and Towers
Miami Beach, Florida

Analysis of Frequency-Domain Optical Mammograms Using Spectral Information

E. Heffer, M.A. Franceschini,
Electro-Optics Technology Center, Deperatment of Electrical Engineering and Computer Science, TuftsUniversity, Medford, MA 02129
Phone: (617) 627-3136, Fax: (617) 627-3151, e-mail:eheffe01@tufts.edu

O. Schütz, H. Siebold
Martin Luther Universitaet Halle/Wittenberg, Institut für Diagnostiche Radiologie Und CT, Halle, Germany

S. Heywang-Köbrunner, L. Götz, A. Heinig
Siemens Medical Technology, Erlangen, Germany

S. Fantini
Electro-Optics Technology Center, Deperatment of Electrical Engineering and Computer Science, TuftsUniversity, Medford, MA 02129

Abstract: Clinical trials of frequency-domain optical mammography have shown promising results giving a sensitivity of 76% and a specificity of 52%. The sensitivity of this method is further investigated by analyzing all false negative results. Specificity can be improved using spectral information.
©1999 Optical Society of America
OCIS codes: (170.0170) Medical optics and biotechnology, (110.0110) Imaging systems, (170.4580) Optical diagnostics for medicine, (170.3830) Mammography, (110.7050) Turbid media

1. Introduction

Frequency-domain optical mammography using edge correction algorithms has produced promising results for the detection of breast cancer in initial clinical trials. The reported sensitivity and specificity for a clinical population of 130 in these trials were 76% and 52%, respectively. There are two objectives in this further investigation of the data: (1) to assess the sensitivity of the method more carefully, meaning to report a study of the false negative results, and (2) to improve the specificity by taking advantage of spectral measurements.

2. Summary

The prototype for frequency-domain optical mammography is comprised of four laser diodes emitting four different wavelengths (690, 750, 788, and 856 nm), used as optical sources that are modulated at an RF frequency of 70 MHz. The source and detector fibers are located on opposite sides of the breast, which is slightly compressed between two parallel glass plates. A planar-tandem scan is then performed and the amplitude and phase information obtained is used to create a two-dimensional projection image of the breast. Two views of the same breast (craniocaudal and oblique) are always acquired. Because the thickness of the breast is variable, (i.e. it is thicker in the center than at the edges between two parallel plates), an edge correction algorithm, using the parameter, N, was used to improve image contrast. The N parameter uses the amplitude and phase information at each pixel, (x,y) as follows:

$$N(x,y)=r_0 ac_0/r(x,y)ac(x,y) \qquad (1)$$

where r_0 is the geometrical separation of the compression plates, ac_0 is the ac amplitude at a pixel where the breast thickness is r_0, $ac(x,y)$ is the amplitude measured at pixel (x,y), and $r(x,y)$ is the breast thickness estimated in the selected pixel using the phase information. [1]

Initial analysis of these images for tumor detection was based on three criteria mentioned in [2]:

1. There is a region of higher absorption appearing in the craniocaudal and oblique views of the same breast;

2. The locations of suspicious regions in craniocaudal and oblique views are consistent with each other;

3. The morphology of the suspicious region is not thread-like in at least one view of the breast. The thread-like appearance is indicative of blood vessels, which would absorb light at the wavelengths being used.

The results of this analysis were then compared with x-ray mammography data, as well as biopsy information and pathology reports in order to determine which results were false positive, false negative, true positive or true negative. In order to improve the sensitivity of the optical method, it is necessary to reduce the number of false negative results, and in order to improve the specificity it is necessary to reduce the number of false positive results.

It has been determined that false results may have several different causes. First, some of the images to be analyzed showed common patterns that likely resulted from geometrical effects. This geometrical pattern made it difficult to determine whether there was actually an absorbing body within the breast or not. In order to correct for this, we introduce a correction factor for the inter-subject variability of the ac dependence on thickness. This modifies the value for the N parameter, resulting in N-images with less evident geometrical patterns.

Second, there were several cases in which a tumor appeared in one view, but not in the other. The reason for this is not yet known, but we believe that it is related to the tumor depth and to geometric effects. Another cause of false results is the third criterion listed above, whose analysis is subjective. An objective identification of blood vessels in the optical mammograms would reduce the subjectivity.

In several of the cases where a false negative result was previously reported, the tumor was located very close to the chest wall and it was outside of the field of view.

One method of reducing the number of false positive results is to use spectral information in order to discriminate among blood vessels, benign lesions, and malignant tumors. It has been observed that the absorption properties of blood vessels differ from those of tumors. While it is yet to be determined whether there is a consistent difference in the spectral properties of malignancies and benign tumors, encouraging results in this direction have been reported.[3]

3.   References

M.A. Franceschini, K.T. Moesta, S. Fantini, G. Gaida, E. Gratton, H. Jess, W.W. Mantulin, M. Seeber, P. Schlag, M. Kaschke, "Frequency-domain techniques enhance optical mammography: Initial clinical results" Proc. Natl. Acad.Sci. USA, 94, 6468-6473, (June 1997)

S. Fantini, O. Schütz, J. Edler, S. Heywang-Köbrunner, L. Götz, M.A. Franceschini, H. Siebold, "Clinical Applications of Frequency-Domain Optical Mammography"Proc. SPIE, 3566, 194-199, (1999)

S. Zhou, S. Huang, C. Xie, H. Long, S. Nioko and B. Chance, "Optical imaging of breast tumor by using dual wavelength amplitude cancellation system (phased array)", Advances in Optical Imaging and Photon Migration, XXI, 294-296, (1998)